Biodiversity responses to Lateglacial climate change in the subdecadally-resolved record of Lake Hämelsee (Germany)

S. Engels [a,b,*], C.S. Lane [c], W.Z. Hoek [d], I. Baneschi [e], A. Bouwman [f], E. Brogan [g], C. Bronk Ramsey [h], J. Collins [i], R. de Bruijn [j], A. Haliuc [k], O. Heiri [l], K. Hubay [m], G. Jones [n], V. Jones [g], A. Laug [o], J. Merkt [p], F. Muschitiello [c], M. Müller [q], T. Peters [b], F. Peterse [f], A. Pueschel [g], R.A. Staff [r], A. ter Schure [b,s], F. Turner [o], V. van den Bos [b,t], F. Wagner-Cremer [d]

[a] School of Social Sciences, Birkbeck University of London, London, WC1E 7HX, UK
[b] Institute for Biodiversity and Ecosystem Dynamics, University of Amsterdam, Science Park 904, 1090 GE, Amsterdam, the Netherlands
[c] Department of Geography, University of Cambridge, Downing Place, Cambridge, CB2 3EN, UK
[d] Department of Physical Geography, Utrecht University, Princetonlaan 8a, 3584 CB, Utrecht, the Netherlands
[e] Institute of Geosciences and Earth Resources IGG, National Research Council of Italy, Pisa, Italy
[f] Department of Earth Sciences, Utrecht University, Princetonlaan 8a, 3584 CB, Utrecht, the Netherlands
[g] Environmental Change Research Centre, Department of Geography, University College London, UK
[h] Research Laboratory for Archaeology and the History of Art, University of Oxford, Dyson Perrins Building, South Parks Road, Oxford, OX1 3QY, UK
[i] Section 5.1 Geomorphology, Organic Surface Geochemistry Laboratory, GFZ German Research Centre for Geosciences, Potsdam, D-14473, Germany
[j] Geological Survey of the Netherlands, Postbus 80015, Utrecht, 3508 TA, the Netherlands
[k] Department of Geography, Faculty of History and Geography, Stefan cel Mare University of Suceava, Romania
[l] Geoecology, Department of Environmental Sciences, University of Basel, Klingelbergstrasse 27, CH-4056, Basel, Switzerland
[m] Institute for Nuclear Research, 4001, Debrecen, P.O. Box 51, Hungary
[n] Department of Geography, College of Science, Swansea University, Singleton Park, Swansea, SA2 8PP, UK
[o] Institute for Geosystems and Bioindication, Technische Universität Braunschweig, Braunschweig, D-38106, Germany
[p] Ritter-Eccartstr 5, Herbertingen, D-88518, Germany
[q] Institute of Geobotany, Leibniz Universität Hannover, Hannover, D-30167, Germany
[r] Scottish Universities Environmental Research Centre (SUERC), University of Glasgow, Rankine Avenue, Scottish Enterprise Technology Park, East Kilbride, G75 0QF, UK
[s] Centre for Ecological and Evolutionary Synthesis, Faculty of Mathematics and Natural Sciences, University of Oslo, Postboks 1066 Blindern, 0316, Oslo, Norway
[t] GNS Science, Lower Hutt, 5010, New Zealand

ARTICLE INFO

ABSTRACT

Anthropogenically-driven climate warming and land use change are the main causes of an ongoing decrease in global biodiversity. It is unclear how ecosystems, particularly freshwater habitats, will respond to such continuous and potentially intensifying disruptions. Here we analyse how different components of terrestrial and aquatic ecosystems responded to natural climate change during the Lateglacial. By applying a range of analytical techniques (sedimentology, palaeoecology, geochemistry) to the well-dated sediment archive from Lake Hämelsee (Germany), we show evidence for vegetation development, landscape dynamics and aquatic ecosystem change typical for northwest Europe during the Lateglacial. By particularly focussing on periods of abrupt climate change, we determine the timing and duration of changes in biodiversity in response to external forcing. We show that onsets of changes in biodiversity indicators (e.g. diatom composition, *Pediastrum* concentrations) lag changes in environmental records (e.g. loss-on-ignition) by a few decades, particularly at the Allerød/

Younger Dryas transition. Most biodiversity indicators showed transition times of 10–50 years, whereas environmental records typically showed a 50–100 year long transition. In some cases, transition times observed for the compositional turnover or productivity records were up to 185 years, which could have been the result of the combined effects of direct (e.g. climate) and indirect (e.g. lake stratification) drivers of ecosystem change. Our results show differences in timing and duration of biodiversity responses to external disturbances, suggesting that a multi-decadal view needs to be taken when designing effective conservation management of freshwater ecosystems under current global warming.

1. Introduction

Anthropogenic climate warming and land use change are affecting ecosystem functioning to a degree that threatens the resilience of the Earth system (Rockström et al., 2009; Steffen et al., 2015). As a result, we are currently observing dramatic changes in the structure and composition of biological communities across all spatial scales, from local to global (Ripple et al., 2017). There is growing evidence for a decrease in global biodiversity, where freshwater habitats show a particularly high rate of biodiversity loss (Dudgeon et al., 2006).

Whilst reliable forecasts exist for e.g. future developments of anthropogenic climate change (IPCC, 2021), much is still unclear on how natural ecosystems will respond to such ongoing and potentially intensifying disruptions. For instance, it is unclear how fast different parts of the ecosystem will respond to external changes such as climate warming or land use change, how long it will take for new equilibria to be reached, and whether there is, e.g., an offset in response rates between terrestrial and aquatic ecosystems. Such information is, however, of key importance for effective conservation management and ecological restoration (Manzano et al., 2020).

Palaeoecological records, particularly those covering time intervals with dynamic external forcing such as abrupt climate change, can provide new insights into the complex relationships that exist between environmental variability and ecosystem functioning (Willis and Birks, 2006; Gregory-Eaves and Beisner, 2011; Birks et al., 2016a; Engels et al., 2020). Many detailed palaeoecological records are now available that combine proxies reflecting terrestrial and aquatic ecosystem response to climate change, using data derived from a single record (e.g. Słowiński et al., 2017; Müller et al., 2021). Such records can be used to infer changes in taxon richness and diversity for both terrestrial and aquatic ecosystems (e.g. Birks et al., 2016b; Engels et al., 2020), changes in community composition (Smol et al., 2005), and changes in past productivity or biomass (Matthias and Giesecke, 2014). These aspects are of key importance to assess overall ecosystem response to external forcing. However, to our knowledge, only Birks et al. (2000) reconstructed changes in biodiversity metrics of both terrestrial and aquatic communities in response to climate change during the Last Glacial-Interglacial Transition period, using data derived from a single record (Lake Kråkenes, Norway). This lack of detailed reconstructions impedes our understanding of biodiversity dynamics in response to abrupt climate change.

The Last Glacial-Interglacial Transition period (LGIT; ca 15-11 cal ka BP) represents a time interval of major climate fluctuations in the Northern Hemisphere (Turney et al., 2006), driven by changes in solar insolation and complex feedback mechanisms between meltwater release, and oceanic and atmospheric circulation processes (McManus et al., 2004; Steffensen et al., 2008; Rach et al., 2014). Some of the most notable climate transitions in northwest Europe during the LGIT include the transition from the Bølling/Allerød (B/A) interstadial to the Younger Dryas (YD) stadial at ca. 12,850 cal a BP (Rasmussen et al., 2014), and the abrupt increase in temperatures that characterises the onset of the current interglacial, the Holocene (ca. 11,650 cal a BP; Walker et al., 2008; Rasmussen et al., 2014). Both these transitions were characterised by changes in summer temperatures in northwest Europe of a 3–4 °C magnitude (Brooks and Langdon, 2014; Heiri et al., 2014), which is similar to the warming forecast between now and the year 2100 CE by

the IPCC (2021)'s SSP3-7.0 scenario. The LGIT therefore provides an ideal scenario for studying biodiversity responses to climate change.

To improve our understanding of regional climate dynamics and ecosystem responses to climate change, a network of well-dated high-resolution palaeoenvironmental records is needed (Lowe et al., 2015). Whilst many palaeoenvironmental records exist for, e.g., northwest Europe, importantly, the dating uncertainty of many available records is in the order of several centuries. These large uncertainties preclude the determination of spatiotemporal leads and lags between sites in terms of climate evolution (Reinig et al., 2021), environmental change, and ecosystem dynamics (Wulf et al., 2016; Słowiński et al., 2017; Engels et al., 2022). Even in a well-studied region such as northwest Europe, only a select number of sites combine a robust independent chronological framework established through, e.g., tephrochronology, varve counting and radiocarbon dating with a range of palaeoecological proxy data (e.g. Trzechowskie (Słowiński et al., 2017), Kråkenes (Birks and Birks, 2013)). These, and other, similar, sites have enabled the determination of leads and lags in the response of different parts of the ecosystem to external forcing (e.g. climate change) with great precision. However, a detailed analysis of the response of key parameters of biodiversity change to climate forcing is currently lacking.

The sediment record of Lake Hämelsee (northwest Germany; Fig. 1) spans from the end of the last glacial to the present and is characterised by a relatively thick sediment interval of LGIT age (Merkt and Müller, 1999). Engels et al. (2022) produced a detailed and robust chronological framework for a new sediment record derived from Lake Hämelsee, making this site an ideal target for the high-resolution analysis of past changes in biodiversity. In this study we use a range of palaeoenvironmental and palaeoecological techniques to.

(a) Reconstruct LGIT climate change and environmental dynamics at Lake Hämelsee, with a specific focus on periods of abrupt change between ca. 14,500 and 10,500 cal a BP.

(b) Determine the timing and duration of changes in biodiversity of both terrestrial and aquatic ecosystems in response to abrupt climate and environmental change.

2. Materials and methods

2.1. Site description, field work and core handling

Lake Hämelsee (52.76 °N, 9.31 °E, 20 m a.s.l.) is located in the northwestern part of Germany, ca. 50 km northwest from the city of Hanover. Due to its proximity to the Atlantic Ocean, the area around Lake Hämelsee is directly influenced by changes in North Atlantic circulation patterns and the westerlies, which are suggested to have been important drivers of LGIT climate change (e.g. Merkt and Müller, 1999; Brauer et al., 2008; Lane et al., 2013). The sedimentary archive of the lake was previously studied by Merkt and Müller (1999), who provided a first detailed account of the Lateglacial vegetation development in the area. They showed that at least two tephra horizons were present in the LGIT section of the lake sediment sequence, and that part of the record consisted of varves, indicating the potential to develop a robust chronological framework for the site. Second, Merkt and Müller (1999) showed that the sediment body spanning the LGIT was relatively thick compared to similar nearby sites (e.g. Lake Hijkermeer; Heiri et al.,

2007) and would therefore offer the opportunity to perform high-resolution palaeoecological and geochemical analyses.

The area around Lake Hämelsee consists of fluvial sands of the Weser/Aller River and major geomorphologic features in the region most likely formed during the late Weichselian (Meinke, 1992; Merkt and Müller, 1999). The origin of the lake is contested; the lake could have developed in a pingo-remnant formed when ice lenses and permafrost disappeared after the onset of the Lateglacial. Alternatively, the lake could have formed as a dolina after the collapse of underlying salt (Merkt and Müller, 1999). The lake currently measures ca. 300 m along its long axis and is surrounded by a commercial campsite. Where there are no artificial grasslands or sandy beaches, the lake is bordered by beds of reed (*Phragmites australis*) and small pockets of alder, birch, and on drier parts, oak. Water lilies (*Nymphaea alba*) are observed in the shallower parts of the lake.

The bathymetry of the lake was established during fieldwork in July 2013 using a hand-held echosounder. Two parallel overlapping core sequences (HAEM-A and -B) were extruded from the centre of the lake (water depth = 3.4 m) using a 3-m-long UWITEC piston corer deployed from a floating platform. A total of six core segments were retrieved at core location HAEM-A, spanning 0.27–17.90 m sediment depth, reaching into the top of the Pleistocene sands underlying the lacustrine infill of the lake basin. Five core segments were retrieved at location HAEM-B, spanning 1.59–16.10 m sediment depth, with the sequence finishing in laminated sediments dating to the LGIT. The cores were subdivided into 1-m long core segments in the field to enable transport.

In this paper we present results obtained from the LGIT interval of a combined central sediment sequence (Haem13). This master sequence was defined by Engels et al. (2022) following matching of core sequences Haem-A and -B based on visual marker layers, detailed loss-on-ignition (LOI) profiles and lithological descriptions. The Haem13 master sequence combines sections of core with high sedimentation rates and avoids coring gaps or other potential coring artefacts. The data presented in this study is mainly derived from core sequence Haem-B, with only the lowermost part of the sequence (below 1612 cm sediment depth) derived from core sequence Haem-A. Engels et al. (2022) used a pollen record derived from the Haem13 sequence to determine the absolute ages of the pollen-transitions at Lake Hämelsee, and compared these dates to absolute ages derived from other regional records. They showed that there were no spatiotemporal lags in vegetation response to Younger Dryas cooling. In the current paper, we build on the work by Engels et al. (2022) by presenting a wider range of proxy indicators, studying the complete LGIT interval of the Haem13 sequence, and by focussing on the determination of temporal offsets between different environmental indicators and metrics of ecosystem diversity derived from a single core sequence (Haem13).

2.2. Chronology

Engels et al. (2022) presented an age/depth model (HaemChron21) for the LGIT section of the Hämelsee sediment sequence. A Bayesian age-depth (depositional) model was developed in OxCal v4.4 (Bronk Ramsey, 2009) and combines information on five tephra deposits that were reliably correlated to known eruptions (Jones et al., 2018), five AMS ^{14}C dates derived from organic material reflecting atmospheric ^{14}C concentrations and, between 1610 and 1525 cm depth, an 825 ($\pm$5 varves) yr long floating varve chronology that is anchored to the absolute time-scale using the Laacher See Tephra (1559-1557 cm depth;
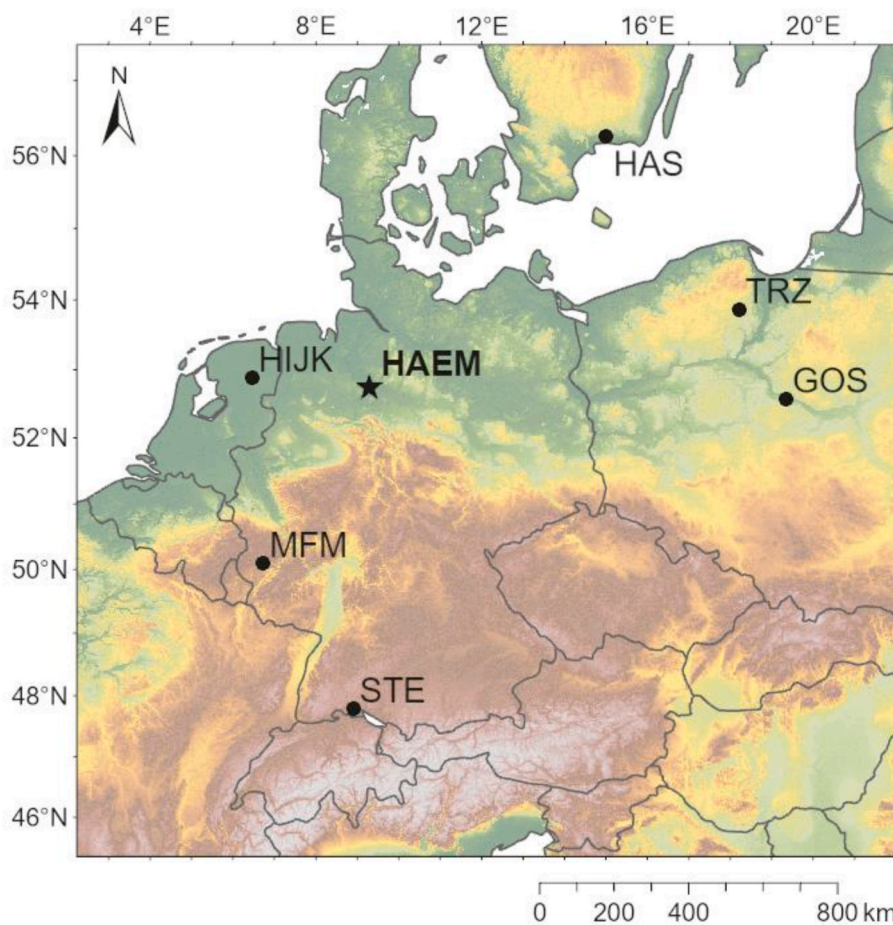
Fig. 1. Map showing the location of Hämelsee (HAEM) and other sites discussed in the text (HAS = Hässeldala, HIJK = Hijkermeer, GOS = Gościąż, MFM = Meerfelder Maar, STE = Steisslingen, TRZ = Trzechowskie). Basemap ©EuroGeographics 2022.

dated to 13,006 ± 9 cal a BP (Reinig et al., 2021)). The full Haem-Chron21 OxCal code is available in Engels et al. (2022) and is here rerun to provide age estimates for the sediment depths corresponding to our sedimentological, palaeoecological and geochemical samples. In this study, calibrated ages are reported in calibrated anni Before Present (cal a BP) with reference to the age/depth model presented in Fig. 2b, with ages rounded to the nearest 5 years.

The age/depth model for the Hämelsee record suggests sedimentation started around 15,000 cal a BP with a lacustrine environment establishing itself from 14,530 cal a BP onward (Fig. 2b). However, age control in the lowermost part of the record relies on only three radiocarbon dates, of which one (sample at 1680-1679 cm depth) is left out of the final model due to poor agreement (Engels et al., 2022). The age/-depth model shows stable and relatively high sedimentation rates throughout the LGIT. The model shows low uncertainty estimates between 13,600 and 12,750 cal a BP as a result of the low (decadal-scale) dating uncertainties associated with the precise age of the Laachser See Tephra (LST) and the varve counting (Reinig et al., 2021; Engels et al., 2022). Outside of this interval, dating uncertainties are of centennial-scale order. However, this study will mainly focus on offsets in changes observed for different indicators obtained from within the Hämelsee record. Therefore, the centennial-scale uncertainties for the non-varved parts of our record will not substantially impact upon our conclusions.

2.3. Sedimentological indicators

Loss-on-ignition was measured on contiguous 1-cm-thick samples taken from both the HAEM-A and HAEM-B sequence to allow for core comparison. Subsamples of 1 cm^3 were dried in an oven at 105 °C for 24 h before being placed in a furnace at 550 °C for 4 h. Loss-on-ignition was calculated by comparing the dry weight of the samples before and after combustion at 550 °C following Heiri et al. (2001) and results are expressed as percentages. The composite LOI record consists of 369 samples and covers the entire LGIT section of the sequence as well as part of the early Holocene (1695.5–1321.5 cm sediment depth; 14,720–8450 cal a BP). The geochemical composition of the sediments was determined on fresh core splits of LGIT and early Holocene age (1687-1325 cm sediment depth; 14,610–8530 cal a BP) using an Itrax X-ray fluorescence (XRF) core scanner equipped with a Cr tube. Measurements were performed at 200 μm resolution during 20s exposure time per step at 30 kV tube voltage and 40 mA tube current (Engels et al., 2022). Selected geochemical major and minor elements (Ti, Si, Ca, Fe) are expressed as log ratio (Log) and centred log-ratios (clr, e.g. Si$_{clr}$) to reduce matrix effects (Weltje and Tjallingii, 2008) and are interpreted to represent local environmental conditions. Ti$_{clr}$ and Si$_{clr}$ are interpreted to represent input of detrital and aeolian materials into the lake basin. Ca$_{clr}$ is interpreted to represent periods of calcite production and deposition. Fe$_{clr}$ is interpreted to indicate periods of stable lake conditions and, potentially, bottom-water anoxia. Log(Ca/Ti) and log(Fe/Ti) ratios are presented to further illustrate changes between periods of stable lake conditions with high in-lake productivity (high values) and periods with unstable conditions and relatively high contributions of allochthonous materials (low values). Thin section analysis was performed for the main purpose of varve identification and counting, and the main results of this analysis are presented in Engels et al. (2022). Additionally, marker layers were characterized throughout the LGIT and early Holocene parts of the record to enable core correlation. Some observations relevant to the palaeoenvironmental reconstruction of the Lateglacial landscape were made during thin section analysis and will be
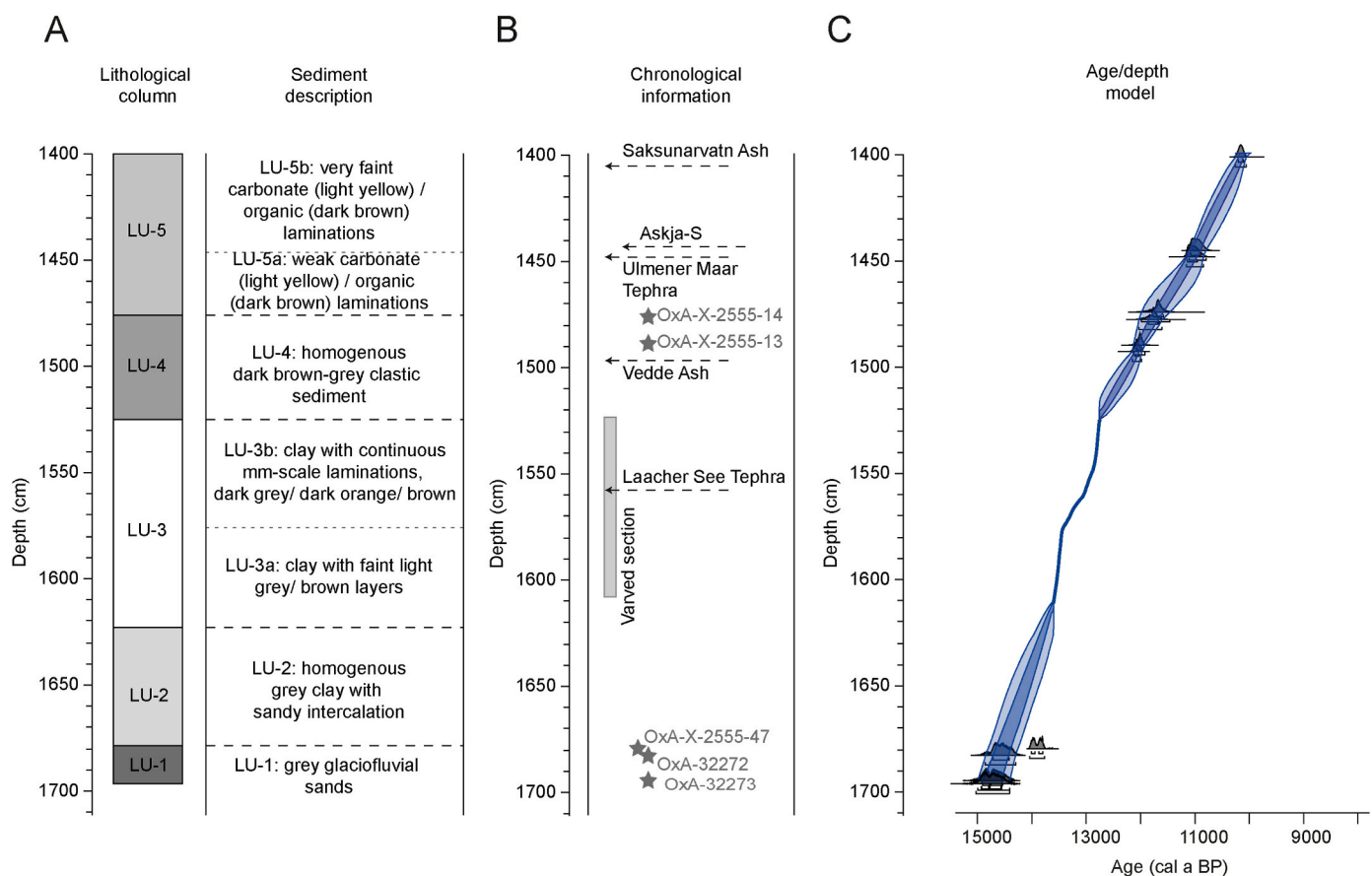

Fig. 2. (A) Lithological column, Lithological Units (LUs) and sediment description; (B) Chronological information, including depths of radiocarbon dates, tephra horizons and varved section; (C) Age/depth model after Engels et al. (2022).

reported here.

2.4. Palaeoecology

Following LOI analysis, Itrax core scanning and sampling for thin section analysis, core segments spanning between 1325 and 1687 cm sediment depth were subsampled into contiguous 1-cm-thick sub-samples. These subsamples formed the basis for the subsequent palae-oecological and geochemical analyses. Engels et al. (2022) selected a total of 126 samples for pollen analysis (1733.5–1413.5 cm sediment depth; 15,220–10,385 cal a BP), with contiguous 1-cm-thick samples selected across the major transitions visible in the sedimentological records of the core. Pollen samples were prepared following standard techniques as described in Faegri and Iversen (1989) and Moore et al. (1991). They were initially boiled in KOH (10%) and subsequently in HCl (10%) and were then sieved through a 212-μm mesh. The samples were dehydrated using 96% acetic acid following washing and centrifuging, and subsequently treated with an acetolysis mixture for 10 min. The samples were washed repeatedly after cooling, and organic and clastic materials were extracted using heavy liquid separation using a bromoform–alcohol mixture. Routine checks of the heavy fraction did not reveal any selective loss of pollen during the separation process. A *Lycopodium* tablet was added to each sample to enable the calculation of pollen accumulation rates (PARs; Stockmarr, 1971).

Results are expressed as a percentage of the total pollen sum, which includes trees, shrubs and upland herbaceous taxa, with encountered pollen taxa assigned to functional groups using the classification developed by Hoek (1997a). If a sample had a pollen sum below 300, it was left out of the final dataset. Our final pollen dataset includes 106 samples, spanning the entire LGIT interval of the Haem13 record with an average pollen sum of 472 pollen grains per sample (range = 307–849). Sampling resolution averages 5 cm per sample in the lowermost part of the record (i.e. below 1600.5 cm sediment depth; before 13,540 cal a BP) except for the large jump (ca. 60 yr.) from the lowermost sample at 15,220 cal a BP to the next, which was the result of sample amalgamation due to low count sums. Apart from regions where samples had to be amalgamated due to low count sums, the sampling resolution is 1 or 2 cm per sample for the remainder of the record, except for a section within the YD where the sampling resolution is 2–4 cm per sample (1511.5–1495.5 cm sediment depth; 12,470–12,130 cal a BP).

Pollen Accumulation Rates (PARs) were calculated by first multiplying the number of encountered pollen grains per taxon by the ratio of the number of *Lycopodium* spores added during laboratory preparation relative to the number of spores encountered during microscope analysis (Engels et al., 2022). The resulting number was then corrected for the surface area of the pollen sample and the number of years included in each sample (as derived from the age/depth model). PARs are presented as the number of palynomorphs per cm^2 per year.

Whilst several biostratigraphical classification schemes exist for northwest Europe in general, and for Germany specifically (Litt and Stebich, 1999), we here follow the biostratigraphical definitions proposed by Hoek (1997a, 1997b) as they pertain to sites on well-drained glaciofluvial deposits similar to Hämelsee and have been developed using a large number of sites all situated close to Lake Hämelsee. Additionally, the term 'Younger Dryas' has been used to indicate a lithostratigraphical, geochronological or a biostratigraphical unit (Mangerud, 2021). We herein define the Younger Dryas as the youngest biostratigraphical LGIT zone characterised by the occurrence of sub-Arctic flora in northwest Europe (Engels et al., 2022). Whereas Engels et al. (2022) focussed exclusively on the biostratigraphic definition and the expression of the onset and end of the Younger Dryas at Lake Hämelsee and beyond, we here use the palynological data to reconstruct terrestrial vegetation development and to reconstruct Late-glacial ecosystem dynamics and biodiversity (pollen diversity, assemblage composition, and productivity) response to climate forcing.

The palynological samples were further analysed to determine the composition of their *Pediastrum* assemblages. Subfossil remains of *Pediastrum* can be identified to subspecies levels and identification of the *Pediastrum* taxa mainly followed Komárek and Jankovská (2001) with further taxonomic revisions as summarised in Turner et al. (2014). Our final *Pediastrum* dataset includes 99 samples, as samples with fewer than 25 identified *Pediastrum* coenobia were excluded from further analyses (cf. Turner et al., 2014, 2016). The *Pediastrum* record covers 1674.5–1419.5 cm sediment depth (14,450–10,495 cal a BP) and has a 2 cm sampling resolution throughout most of the sequence, with higher sampling resolution (1 cm) around the major transitions observed in the record, and with lower sampling resolution (3–12 cm) in the lowermost part of the record (below 1600.5 cm; before 13,540 cal a BP). *Pediastrum* concentrations were calculated by comparing the number of *Lycopodium* spores encountered during analyses to the number of spores added to the sample.

A total of 78 samples were selected for diatom analysis at 2–5 cm intervals (1571.5–1412.5 cm; 13,340–10,365 cal a BP), with a higher sampling resolution (contiguous 1 cm intervals) around key transitions. Organic matter was removed from the samples (ca. 0.01 g dried sediment) by oxidation using 5 ml of H_2O_2 (30%) and heating in a water bath at 70 °C for 24–28 h. Subsequently, a few drops of HCl (50%) were added to remove residual H_2O_2 and carbonates. Samples were washed by adding distilled water, shaking vigorously, centrifuging at 1200 rpm for 4 min, and removing the liquid using a pipette. This process was repeated 5 times, and a few drops of ammonia (NH_3) were added to the solution prior to the final wash to prevent clumping of diatoms. Approximately 0.5 ml of diatom suspension was placed onto clean coverslips and left to dry at room temperature before mounting the slides using Naphrax. Diatoms were identified using a light microscope at 1000× magnification and mostly identified using Krammer and Lange-Bertalot (1986–1991) and Camburn and Charles (2000). Nomenclature was updated with AlgaeBase (Guiry and Guiry, 2024) Taxa were identified to species level, however diatoms that could not be identified to species level due to poor preservation, damage, or deformation, or those that were too rare to justify detailed taxonomic work, were identified to genus level (e.g. *Eunotia* sp.). For several samples the target count sum of 300 diatom valves could not be reached due to low concentrations or poor diatom preservation. Where possible, neighbouring samples with a low count sum were amalgamated until a count of at least 100 valves was reached; if this was not possible (e.g. with subsequent samples having no diatoms preserved) the samples were deleted from our dataset prior to analysis. This process resulted in a final diatom dataset including 57 samples (average count sum = 231 valves, range = 100–308 valves). We use shortened names for diatom taxa in this manuscript and refer to Supplementary Table SI1 for the full scientific names.

A total of 123 samples were analysed for subfossil chironomid remains between 1721.5 and 1417.5 cm sediment depth (15,060–10,460 cal a BP), where sampling in the first instance used a coarse resolution (4–6 cm per sample) followed by a second round of sample selection focussing on parts of the sequence that showed community dynamics. The samples were treated with warm KOH (10%) for 10–20 min to de-flocculate the material and subsequently rinsed through a sieve with a 100-μm mesh. Chironomid head capsules (HCs) were hand-picked from the residue using a Bogorov sorting tray and mounted on permanent microscope slides using Euparal mounting medium. HCs were identified using Brooks et al. (2007) and the dataset presented here has been matched to the taxonomy of the merged Norwegian/Swiss chironomid-climate calibration dataset (Heiri et al., 2011). Specimens that could not be identified beyond subfamily or tribe level due to, e.g., missing mouth parts were removed prior to further analysis. Similarly, a small number of rare taxa that were present in the fossil dataset but absent from the calibration dataset (e.g. *Propsiloceros lacustris*-type) were excluded from the chironomid dataset. Several samples had low chironomid concentrations and for these we amalgamated adjacent samples (within lithological boundaries) to reach a minimum count sum

of 50 head capsules per sample (e.g. Heiri and Lotter, 2001). This process resulted in a final chironomid dataset containing 97 samples (average count sum = 83 HCs, range = 50.5–214.5 HCs). The final chironomid record contains consecutive samples across the onset (1551.5–1536 cm sediment depth; 12,930–12,795 cal a BP) and end of the YD (1495.5–1476.5 cm sediment depth; 12,130–11,750 cal a BP) and a lower sampling resolution in the other parts of the record.

As temperature was believed to be the primary driver of changes in the fossil chironomid data, Engels et al. (2022) used the 274-lake Norwegian-Swiss dataset (Heiri et al., 2011) to quantitatively infer past July air temperatures (T_{jul}) from the data. The calibration dataset was selected based on its proximity to our fossil site, its similarity in climate regime to our site for reconstruction, and the long temperature gradient covered by the dataset spanning 3.5–18.4 °C July air temperature (Heiri et al., 2011). We herein present a number of methods that test the reliability of the chironomid-inferred temperature (CI-T) record presented in Engels et al. (2022). These include the determination of the abundance of fossil taxa that are rare in the calibration dataset, the identification of subfossil samples with no near modern analogues and the goodness-of-fit to the temperature gradient (see Birks et al. (1990) and Engels et al. (2010) for more detail and examples).

Percentage-abundance diagrams were constructed for the pollen, *Pediastrum*, diatom and chironomid records using C2 (Juggins, 2007). The chironomid-based temperature reconstruction and the reconstruction diagnostics calculations were performed in Rstudio version 1.3.1073 (RStudio Team, 2020) using the 'rioja' (Juggins, 2017) and 'analogue' (Simpson, 2020) packages.

2.5. Geochemical analysis

A total of 167 samples spanning the LGIT and early Holocene sections of the cores (1584.5–1412.5 cm sediment depth; 13,470–10,370 cal a BP) were processed using a Dionex 350 accelerated solvent extraction (ASE) system. Solid phase extraction (SPE), using the manual method described in Rach et al. (2020), was used to separate the extracts into an aliphatic, aromatic and alcohol/fatty acid fraction. Separation was achieved by loading the extracts on activated silica columns and eluting each fraction with hexane, hexane/DCM (1:1 v/v) and DCM/MeOH (9:1 v/v) successively. The aliphatic fraction, containing the *n*-alkanes, was analysed by gas chromatography-mass spectrometry (GC/MS). The peak areas for each *n*-alkane homologue were compared to the peak areas from an internal standard (5α-androstane) and an external *n*-alkane standard mixture for absolute quantification. We refer to Rach et al. (2020) for further details on the exact analytical setup. Average chain length (ACL) and the carbon preference index (CPI) of the sediment samples were determined to estimate origin and preservation condition (Allen and Douglas, 1977; Jansen et al., 2008).

Prior to isotope ratio measurement, the aliphatic fraction was further fractionated on a Pasteur pipette column containing activated $AgNO_3$ (10%) coated silica gel. Compound-specific hydrogen isotope ratios (expressed as δD) were subsequently measured on an isotope ratio mass spectrometer. All δD values are normalised to the Vienna Standard Mean Ocean Water (VSMOW) scale using a linear regression function between measured and certified δD values of a standard mix. We refer to Van den Bos et al. (2018) and Rach et al. (2020) for a more detailed description of the methods used to analyse the *n*-alkane biomarkers and compound-specific hydrogen isotope ratios. The hydrogen isotopic composition of plant waxes from woody terrestrial plants, the main source of long-chained *n*-alkanes, reflects that of the source water used by the plants for lipid synthesis. The isotopic composition of the source water is ultimately linked to the isotopic composition of meteoric water, and thus hydrological conditions (see Sachse et al., 2012 for a review). We therefore interpret the trends in our δD records as an indicator of past hydrological change (Sachse et al., 2012) and will focus on relative differences within and between the compound-specific δD curves, where more negative δD values are interpreted to represent drier conditions.

The alcohol/fatty acid fraction of the samples used for lipid extraction was further processed to analyse glycerol dialkyl glycerol tetraethers (GDGTs), which are membrane lipids of certain archaea and bacteria (Schouten et al., 2013). The sampling was specifically focussed on the onset and end of the YD period and covers the samples between 1561.5 and 1468.5 cm sediment depth (13,100–11,550 cal a BP), selecting a subset of 94 samples of the 167 samples originally used for lipid extraction to account for limited laboratory availability. In short, a known amount of internal standard was added to each fraction, which was then redissolved in hexane:isopropanol 99:1 and passed over a 0.45 μm PTFE filter prior to injection on a Agilent 1260 Infinity ultra-high performance liquid chromatograph coupled to an Agilent 6130 single quadrupole mass spectrometer following the settings and elution protocol of Hopmans et al. (2016). A minimum peak area of 3000 and a signal-to-noise ratio of >3 was maintained as detection limit. Quantification of the GDGTs is based on the assumption that the mass spectrometer equally responds to the GDGTs and the internal standard.

Engels et al. (2022) calculated the GDGT-0/crenarchaeol ratio using the GDGT concentrations. Whereas crenarchaeol is exclusively produced by Thaumarchaeota, GDGT-0 can have multiple sources. Since the ratio of GDGT-0/crenarchaeol never exceeds 2.0 in Thaumarchaeotal cultures, values > 2 are indicative of the presence of methanogenic *Euryarchaeota* (Blaga et al., 2009; Bechtel et al., 2010). The presence of methanogens is typically linked to anoxic (bottom) water conditions, for example due to reduced mixing of the water column as a result of changes in temperature or windiness. Engels et al. (2022) interpreted changes in the GDGT-0/crenarchaeol ratio as an indicator of lake water oxygenation, which, given the local settings, was likely driven by changes in windiness with lower GDGT-0/crenarchaeol ratios indicating increasing oxygen-rich conditions near the bottom of the lake, likely driven by increased windiness.

We additionally calculated the degree of methylation of 5-methyl brGDGTs, quantified as MBT'$_{5me}$ (Weijers et al., 2007; de Jonge et al., 2014). The MBT'$_{5me}$ is primarily correlated with mean annual air temperature (MAAT) in soils, peats, and lake sediments worldwide (De Jonge et al., 2014; Dearing Crampton-Flood et al., 2020; Martinez-Sosa et al., 2021) and can thus be used to reconstruct past temperature change. We use the latest global lacustrine Bayesian transfer function that translates MBT'$_{5me}$ into the mean temperature of months above freezing (MAF), using a prior mean and standard deviation of 10 °C (Martinez-Sosa et al., 2021). Figures illustrating the results of the biomarker analyses were constructed in C2 (Juggins, 2007).

2.6. Piecewise linear regression

We used piecewise linear regression (PLR; Mudelsee, 2019) to objectively estimate points of change across the Allerød/YD and YD/Preboreal transitions for selected sedimentological, palaeoecological and geochemical records. Where no satisfactory estimates could be obtained for the onset and end of changes in selected proxy records using PLR (Supplementary Table SI2), we use visually established change-points (Supplementary Table SI3). Dates for the onset and end of changes in the terrestrial environment around Lake Hämelsee were determined by applying PLR to the LOI record as well as to the log (Fe/Ti) record, here interpreted as an indicator of sediment source and catchment processes (see below). PLR was additionally applied to selected geochemical records (δD$_{C29}$ and GDGT-0/crenarchaeol) to establish changes in hydroclimate and in lake water oxygenation, respectively.

We explored biodiversity response to changes in the physical environment and climate by analysing trends in: (a) alpha diversity, here defined as the taxon richness of an assemblage at one point in time; (b) compositional turnover; and (c) flux or concentration, as an approximation of changes in past ecosystem productivity. First, trends in taxonomical diversity were derived for each of our palaeoecological datasets by calculating the Shannon diversity index, which is a widely

used diversity parameter that accounts for both abundance and evenness of the species present (e.g. Schmera et al., 2017). The Shannon diversity index was calculated for the pollen sum taxa (pollen dataset) or for all taxa identified (*Pediastrum*, chironomid and diatom datasets) in R using the 'vegan' package (Oksanen et al., 2019) and PLR was applied to each of the Shannon index curves to determine the onset and end of change. Second, we use trends in compositional turnover (CT) as estimated through Detrended Correspondence Analysis (DCA) to approximate community-level responses to external drivers (c.f. Colombaroli and Tinner, 2013; Engels et al., 2020). DCA was performed using 'vegan' in R and PLR was subsequently applied to sample-scores on the first DCA axis for each of our palaeoecological datasets. Third, we analysed temporal trends in productivity as approximated through arboreal pollen and *Pediastrum* accumulation rates, as well as through trends in chironomid concentrations. As no microspheres were added during sample preparation for diatom analysis, we have not been able to calculate diatom concentrations or accumulation rates. All PLR analyses were performed in R using the 'segmented' package (Muggeo, 2008). Our PLR results can be reproduced using the datasets as uploaded to Pangaea (see Data Availability), the example code available in Supplementary Code SI.1 and the sampling intervals as provided in Supplementary Table SI2. Supplementary Table SI2 and SI3 provide detailed results and interpretations of our PLR and visual analyses, and we summarise the main outcomes of the analyses in Table 1 of this manuscript.

3. Results

3.1. Sedimentological indicators

The Haem13 composite sediment record is subdivided into five major lithological units (LUs) based on the sediment composition, macroscopic structures and colour, as well as the presence and structure of laminations. Basal unit LU-1 (1696-1679 cm; 14,720–14,515 cal a BP; Fig. 2) is composed of grey glacio-fluvial sands, which show maxima in Si_{clr} and minima in Ti_{clr} and Fe_{clr} (Fig. 3). LOI values are very low (0–2%) in the bottom part of the record (Fig. 3). A sharp transition to homogenous light grey clay and LOI values of ca. 10% marks the onset of LU-2 (1679-1623 cm; 14,515–13,765 cal a BP). Si_{clr} decreases sharply at the onset of LU-2, whereas the Ti_{clr}, Ca_{clr}, Fe_{clr} and LOI records all show increases at this point. LU-2 generally shows stable values of Ti_{clr} and Si_{clr} but includes a 6 cm thick layer of rounded sand grains. This layer is characterized by a sharp increase in Si_{clr} and an abrupt decrease in Ti_{clr} and Fe_{clr}. The gradual increase in LOI that started at the onset of LU-2 is interrupted at this point, with LOI values decreasing to near 0%, before again showing a gradual increase during LU-2 and continuing into LU-3. We interpret the high Ca_{clr} values observed during LU-2 (as well as in later parts of the record) and the high log(Ca/Ti) values as an indication of in-lake production of calcites, rather than as the result of detrital input. LU-3 (1623-1525 cm; 13,765–12,755 cal a BP) consists of laminated sediments which between 1610 and 1525 cm are interpreted to be of annual origin. Subzone LU-3a (1623-1576 cm; 13,765–13,430 cal a BP) consists of faintly laminated sediments composed of alternating brown organic and light grey clay layers with relatively high Ti_{clr} and Si_{clr} with values comparable to those of LU-2, and with a gradually increasing Fe_{clr} and LOI values. Subzone LU-3b (1576-1525 cm; 13,430–12,755 cal a BP) is composed of dark grey, dark orange and brown millimeter-to submillimeter-scale laminated sediments consisting of siderite, calcite and organic layers. The organic layers mainly consist of amorphous organic matter that we interpret to have settled in quiet waters under ice cover. LU-3b shows a decrease in Ti_{clr} values compared to LU-3a and an increase in Fe_{clr}, indicating a stable lake environment with decreasing allochthonous input. LOI values stabilize during LU-3b and reach maxima of 30%, where Si_{clr} and Ca_{clr} are comparable to values observed during LU-3a. The high log(Fe/Ti) values
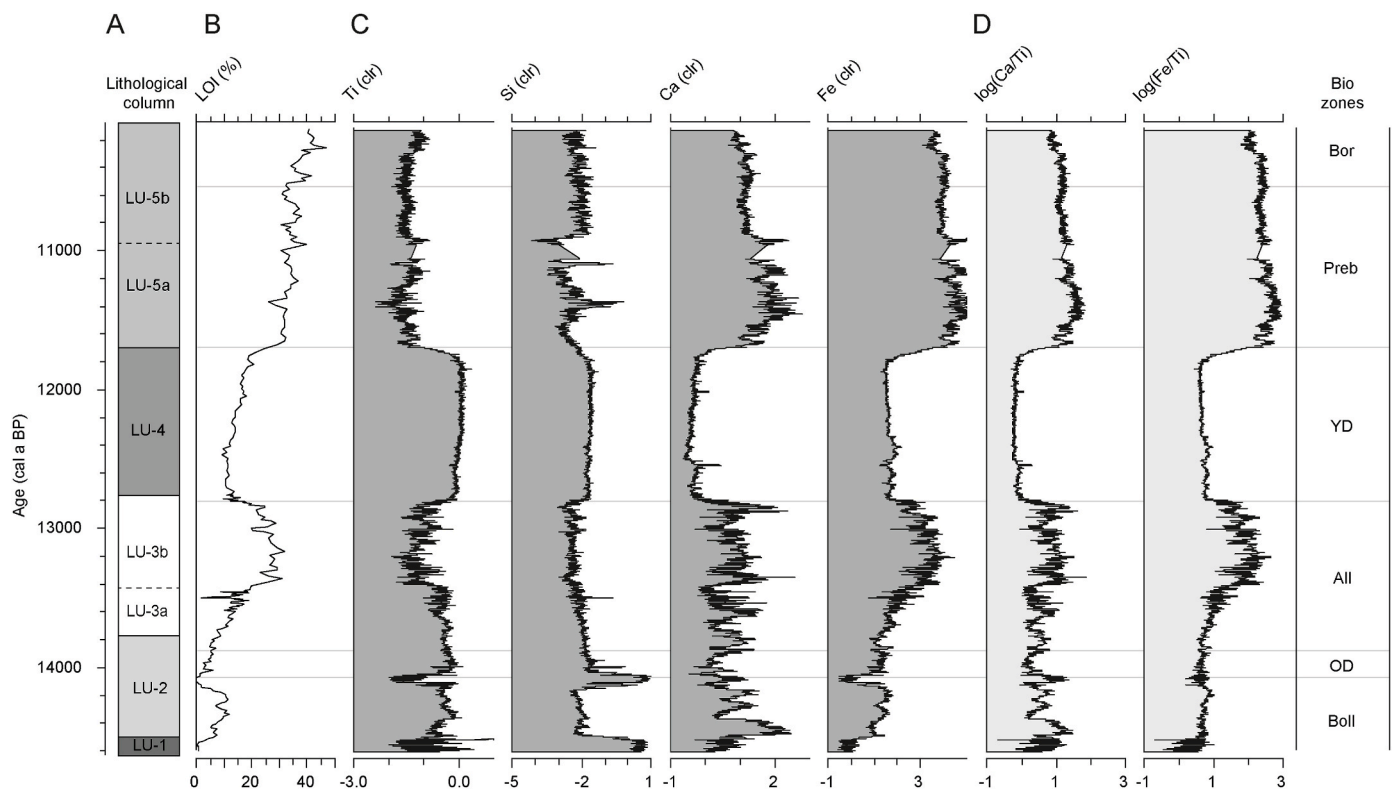
Fig. 3. Sedimentological proxies. (A) Lithological column; (B) Loss-on-ignition record (LOI; %); (C) Selected elements as determined through x-ray fluorescence (XRF) scanning (expressed as centred log ratios (clr)); (D) Elemental ratios. Note the different scales used for the curves in (C). Zonation follows the northwest European classification system for regional biozones (Hoek, 1997a,b) as presented in Engels et al. (2022): Boll = Bølling; OD = Older Dryas; All = Allerød; YD = Younger Dryas; Preb = Preboreal, Bor = Boreal.

during LU-3 are interpreted as an indication of a decrease in detrital input and/or the presence of stable lake conditions, potentially including phases of bottom-water anoxia. LU-3b contains a visible tephra layer that was identified by Jones et al. (2018) as the Laacher See Tephra. LU-4 (1525-1475 cm; 12,755–11,715 cal a BP) is composed of dark brown-grey clastic sediment with lower LOI values, high Ti_{clr} and Si_{clr} values, and low Ca_{clr} and Fe_{clr} values. The combination of low LOI values and high Si_{clr} during LU-4 potentially indicates an increased input of allochthonous material. Log(Ca/Ti) and log(Fe/Ti) both show low values throughout this part of the record, suggesting relatively unstable lake conditions with high detrital input. Faintly laminated dark brown and light-yellow sediments are characteristic for subzone LU-5a (1475-1445 cm; 11,715–10,975 cal a BP), showing carbonate-rich laminae alternating with organic-rich laminae consisting of amorphous organic material. This part of the record shows high LOI, Fe_{clr} and Ca_{clr} values and minima in Ti_{clr} and Si_{clr}. Log(Ca/Ti) and log(Fe/Ti) show sharp increases as well, indicating the re-establishment of stable lake conditions and, potentially, bottom water anoxia. LU-5b (1445-1318 cm sediment depth; 10,975–8450 cal a BP) is composed of dark organic sediments interrupted by faint light carbonate and dark organic layers and shows slightly decreased Fe_{clr} and Ca_{clr} values relative to LU-5a, whereas LOI values continue to gradually increase, reaching maxima of ca. 40%. Several of the zonal boundaries observed in the sedimentary record coincide with major shifts in the pollen diagram (Fig. 3), which form the basis of our palaeoecological interpretations (see below). For instance, the transition between LU-3b and LU-4 coincides with the Allerød/YD biozone transition.

3.2. Palaeoecology

The lowermost section of the Haem13 sequence (below 1674 cm depth; 14,450 cal a BP) showed low pollen concentrations and poor pollen preservation. As a result, no reliable interpretation could be derived for this bottom part of the record. The first lacustrine sediments of the Haem13 sequence contain high *Salix* and *Betula* abundances, indicating deposition during the Bølling biozone (Fig. 4). Increased abundances of Poaceae between 14,070 and 13,880 cal a BP represent the local expression of the Older Dryas, after which the increased PARs

and percent-abundances of *Betula* (60–80%) and then *Pinus* (20–40%) characterise the Allerød interstadial (13,880–12,820 cal a BP). The onset of the YD is reflected by a number of changes in the palynological record (Engels et al., 2022), with first indications of vegetation change around Lake Hämelsee identified at 12,820 cal a BP (Fig. 4) where PARs of, e.g., *Salix* and *Juniperus* show a dramatic drop (Fig. 4b). These changes are followed by a major decrease in *Betula* percent-abundances around 12,800 cal a BP and increases in Poaceae and Non-Arboreal Pollen (NAP). A mid-YD transition is identified at 12,180 cal a BP where *Empetrum* shows an increase in PARs and percent-abundances (>5%). The transition into the Holocene starts when *Empetrum*-PAR starts to decrease from 11,790 cal a BP onward (cf. Engels et al., 2022), which is followed at 11,690 cal a BP by an abrupt increase in *Betula* percent-abundances. The pollen record shows a distinct but temporary increase of Poaceae during the early Holocene (in the figures labelled as Preboreal and, where appropriate, Boreal), characterising the dry and continental Rammelbeek phase as observed in palynological records from across northwest Europe (e.g. Bos et al., 2007). The increase of *Corylus* abundances at 10,550 cal a BP marks the onset of the Boreal at Hämelsee.

The *Pediastrum* record shows very high abundances of *Pseudopediastrum (Pp.) boryanum* var. *boryanum* a (Fig. 5) during the Bølling. During the Older Dryas, *Pediastrum orientale* type A and *Pediastrum integrum* type b increase in abundances and cold-indicating *Pp. kawraiskyi* shows single occurrences (Fig. 5a). The Allerød is characterised by diverse *Pediastrum* assemblages with high abundances of, e.g., *Pediastrum integrum* and *Pp. boryanum* var. *longicorne* and with relatively low concentrations of *Pediastrum* coenobia (Fig. 5b). *Pp. kawraiskyi* shows maximum abundances of >60% during the first half of the YD, before showing a decrease in the second half of the YD. At the onset of the Holocene *Pp. kawraiskyi* disappears completely from the assemblage and *Pediastrum* cf. *angulosum* and *Pediastrum orientale* type a decrease in abundance. *Pp. boryanum* var. *longicorne* reaches maximum abundances of >60% during the Preboreal.

The diatom flora of the late Allerød is characterized by high percentage abundances of *Lindavia bodanica*, *Pantocsekiella ocellata* and needle-shaped *Fragilaria* species (Fig. 6). These planktonic taxa all disappear at the onset of the YD, where benthic taxa that were present in lower abundances during the Allerød (e.g. *Pseudostaurosira brevistriata*,
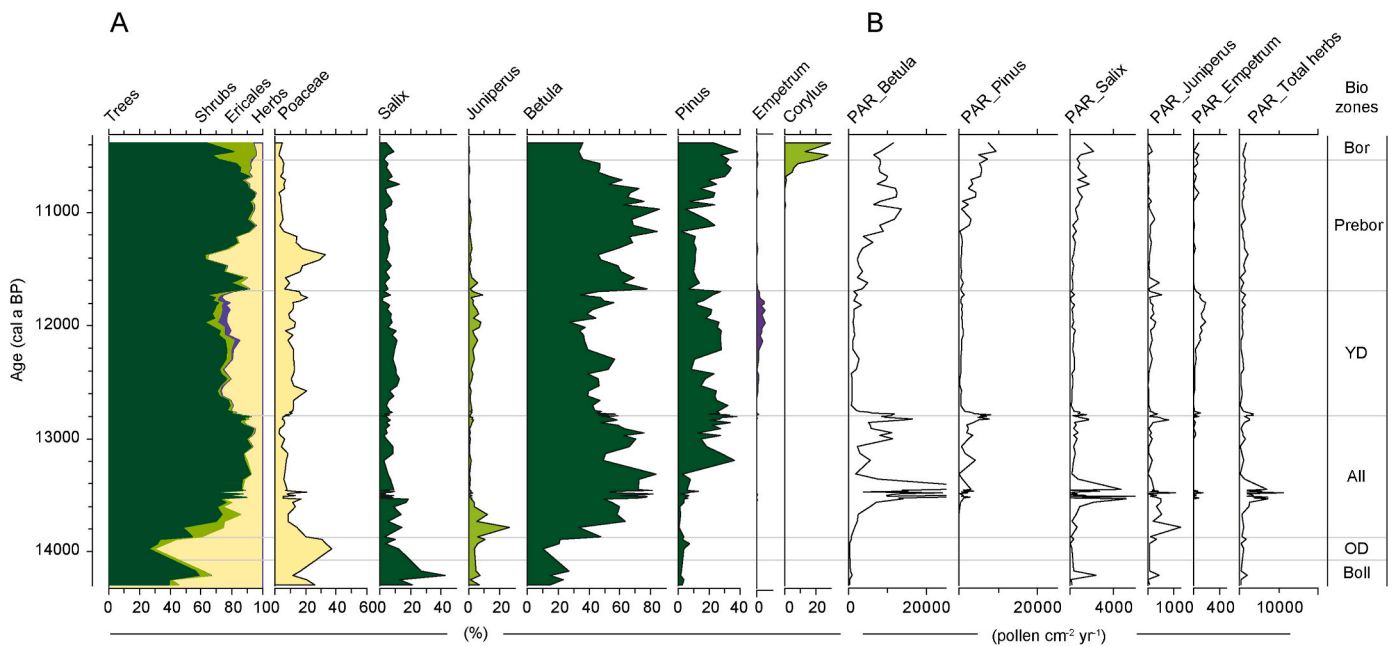
Fig. 4. Pollen record. (A) Selected pollen taxa expressed relative to the Pollen Sum which includes pollen from trees (dark green), shrubs (light green), ericaceous taxa (purple) and upland herbaceous taxa (yellow) (%). (B) Pollen Accumulation Rates (PARs) for selected taxa (pollen cm^{-2} yr^{-1}). Zonation follows the northwest European classification system for regional biozones (Hoek, 1997a,b) as presented in Engels et al. (2022).
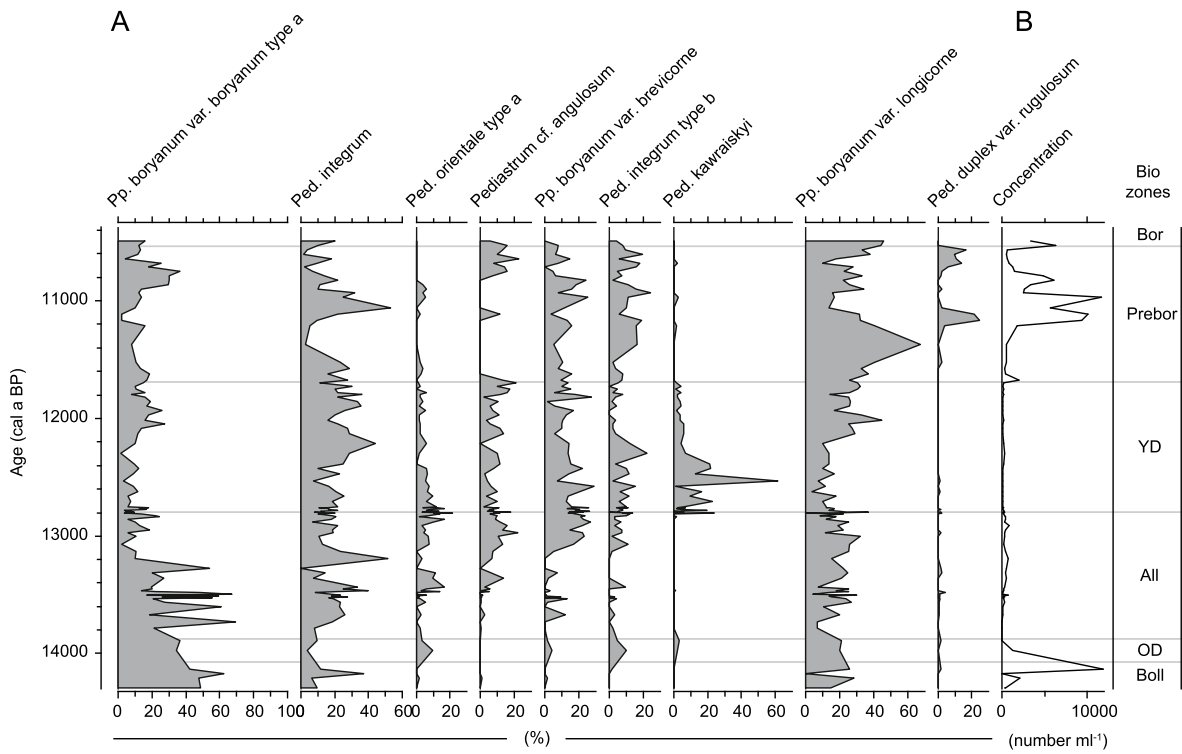
Fig. 5. *Pediastrum* record. (a) Selected *Pediastrum* taxa as a percentage of all coenobia (%); (B) Total *Pediastrum* concentrations (number cm^{-3}). Zonation follows the northwest European classification system for regional biozones (Hoek, 1997a,b) as presented in Engels et al. (2022).
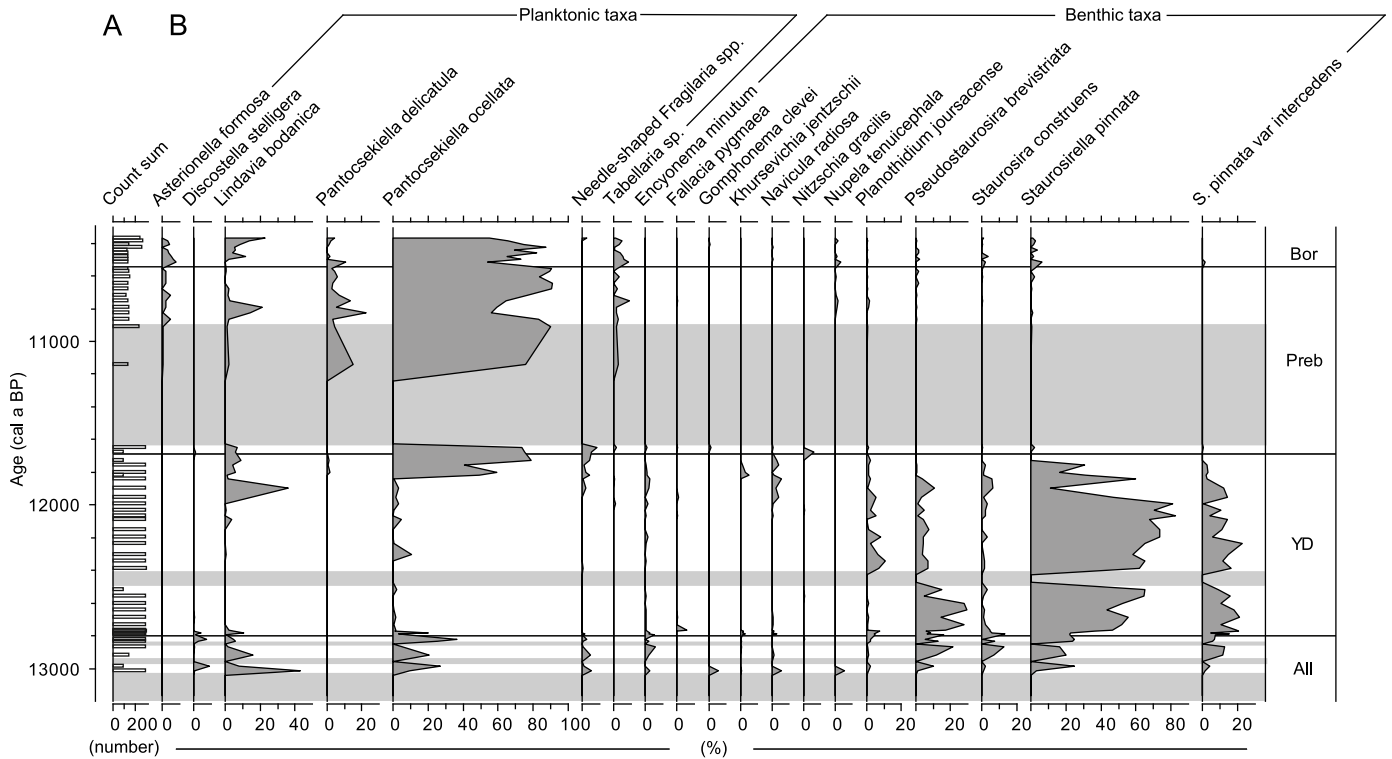
Fig. 6. Diatom record. (A) Diatom count sums (number of valves); (B) Selected diatom taxa expressed as a percentage of all valves (dark grey silhouettes), grouped according to habitat preference. Zonation follows the northwest European classification system for regional biozones (Hoek, 1997a,b) as presented in Engels et al. (2022), light grey blocks indicate parts of the record with poor or no diatom preservation.

Staurosirella pinnata) start to dominate the assemblages. *Staurosirella pinnata* reaches abundances of >60% during the YD, and *Pseudostaurosira brevistriata*, *S. pinnata* var. *intercedens* and *Planothidium joursacense* show maximum abundances during this period. The uppermost samples of the YD show a decline in the abundance of *S. pinnata* and an increase in *Navicula radiosa*. The Holocene is characterized by very low

abundances of almost all benthic taxa, whereas planktonic taxon *P. ocellata* reaching abundances of >80% during the Preboreal. *Asterionella formosa*, several centric taxa and *Tabellaria* sp. are characteristic of the Preboreal and Boreal diatom assemblages, where diatom preservation generally is poor.

The chironomid fauna shows a number of abrupt changes across the LGIT (Fig. 7), generally coinciding with the major transitions as seen in the pollen record. The lowermost samples of the record have very low head capsule concentrations. *Paratanytarsus* spp. shows high abundances in the lowermost two samples, and from 14,490 cal a BP onward, *Corynocera ambigua* and *Microtendipus pedellus*-type characterise the chironomid assemblages of the Bølling interstadial. Cold-indicator *Stictochironomus rosenschoeldi*-type (Brooks et al., 2007) and disturbance-indicator *M. pedellus*-type both reach maximum abundances during the Older Dryas, before disappearing again at the onset of the Allerød interstadial. The Allerød chironomid fauna is diverse and consists mostly of warm-indicating taxa such as *Pagastiella*, *Polypedilum nubeculosum*-type and *Chironomus anthracinus*-type, and includes taxa that are indicative of a profundal habitat (*C. anthracinus*-type, *Tanytarsus lugens*-type). Many of the taxa that are abundant during the Allerød disappear from the assemblages during the Younger Dryas and are replaced by intermediate-to cold-indicating taxa such as *Micropsectra insignilobus*-type and *M. pedellus*-type. The Preboreal biozone shows a decline in the abundance of cold-indicating chironomid taxa in favour of warm stenothermic taxa such as *Dicrotendipes nervosus*-type and *Glyptotendipes pallens*-type (Brooks et al., 2007). The alternations between assemblages dominated by cold- and warm-indicating taxa suggests that climate change was an important driver of the composition of the chironomid fauna.

The chironomid-inferred temperature (C-IT) record shows a dynamic climate across the LGIT. C-ITs are relatively low during the Bølling interstadial and the Older Dryas stadial (ca. 11.5–13.5 °C) and show an increase to values of 14.5–15 °C at the start of the Allerød. The C-IT record shows a decreasing trend during the Allerød though with increased C-ITs observed in the latter part of the biozone. Inferred temperatures drop abruptly to values between 12 and 13 °C at the onset of the Younger Dryas, before showing an increase to values of 14–17 °C during the Preboreal. The reconstruction diagnostics (Supplementary Information Fig. SI1) show that, with the exception of a few individual samples, the fossil assemblages are generally well-represented in the modern calibration dataset and show a good fit to temperature. The percent-abundance of rare taxa generally is low throughout the core. Combined, this suggests that there are no numerical indications that specific parts of the C-IT record should be considered less reliable.

3.3. Lipid biomarker geochemistry

The alkane distribution in a lake sediment sample is a composite of a mix of *n*-alkane homologues derived from different plant species, both aquatic and terrestrial (Sachse et al., 2012). Typically, long-chain alkanes such as C_{27}, C_{29} and C_{31} are interpreted to have mostly been derived from woody species (Rach et al., 2014). By contrast, *n*-alkanes of mid-chain length (C_{23} and C_{25}) in lake sediments are proposed to derive mainly from non-emergent aquatic plant species (Ficken et al., 2000). Concentrations of most individual *n*-alkanes show an increasing trend across the Allerød, interrupted by a decrease to very low concentrations during the late Allerød (Fig. 8a). Concentrations then show a short-lived increase across the Allerød/YD transition, after which the long-chain alkanes (C_{27}, C_{29} and C_{31} homologues) show relatively low concentrations during the first half of the YD. *n*-alkane concentrations of all homologues increase at 12,260 cal a BP, predating the mid-YD transition as observed in the pollen record at 12,180 cal a BP. All *n*-alkane concentration records show a decrease at the onset of the Preboreal. A carbon preference index of >5 indicates that degradation rates were low and

Fig. 7. Chironomid record. (A) Chironomid count sums (number of head capsules (hcs)) and chironomid concentrations (hcs/g); (B) Selected chironomid taxa expressed as a percentage of all identified head capsules (%); (C) Chironomid-Inferred July air Temperature record (C-IT; °C) with sample-specific error estimates. Zonation follows the northwest European classification system for regional biozones (Hoek, 1997a,b) as presented in Engels et al. (2022).

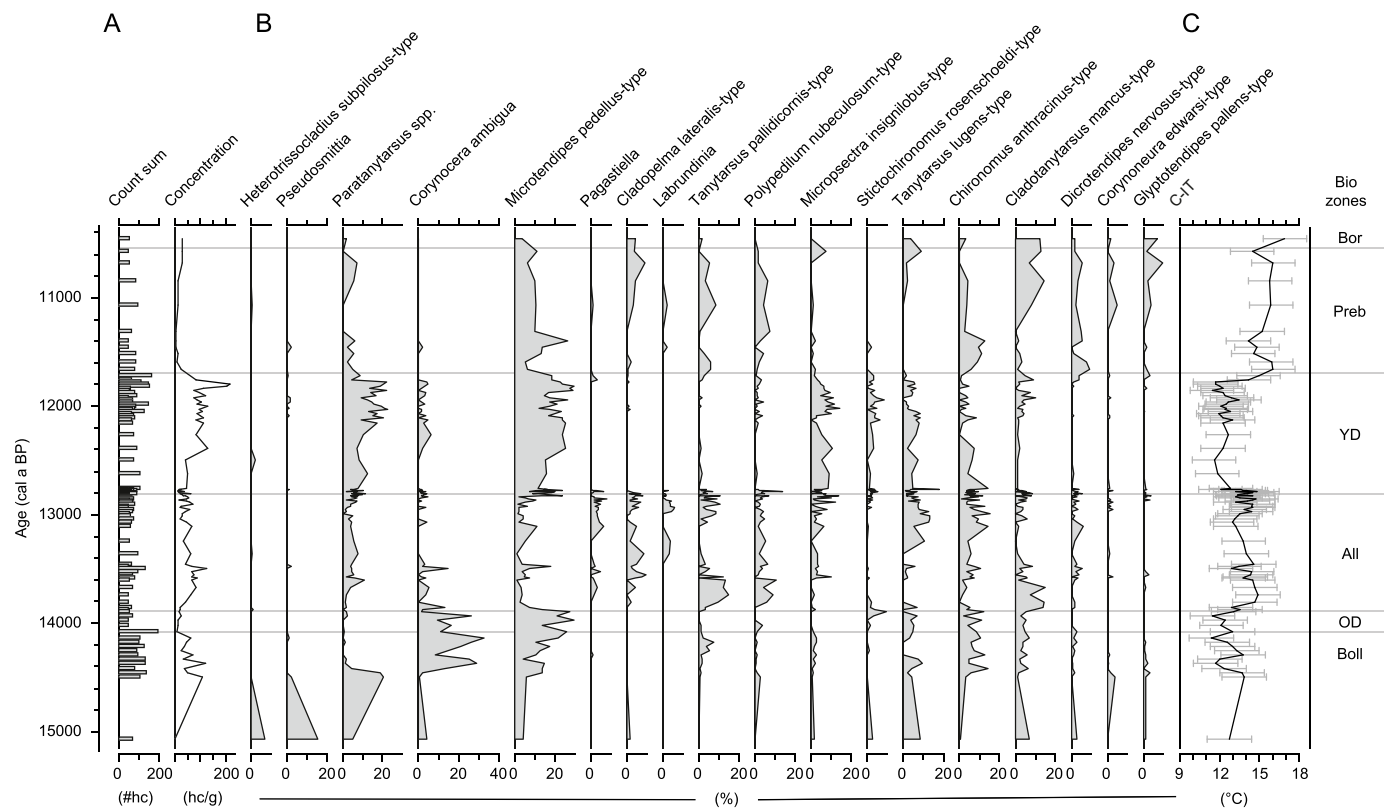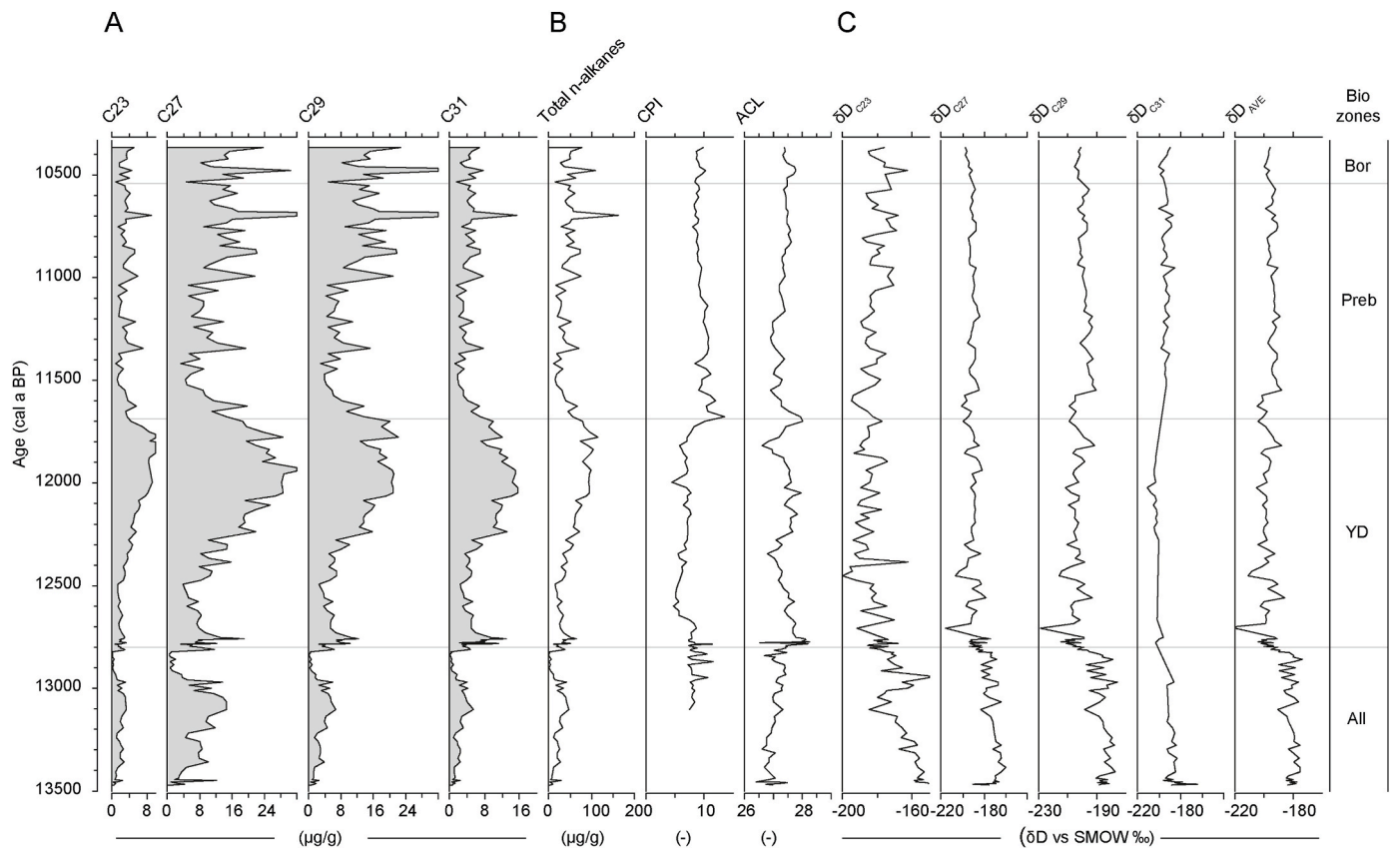**Fig. 8.** *n*-Alkane record. (A) Concentrations of selected *n*-alkanes (μg/g dry weight); (B) *n*-Alkane summary records: Total n-alkane concentration (μg/g dry weight), Carbon Preference Index (CPI) and the Average Chain Length (ACL); (C) Hydrogen isotopic ratios (δD values) of C_{23}, C_{27}, C_{29}, C_{31} and the average δD value of the long-chain alkanes (C_{27}–C_{31}). Note the individual x-axes used for each graph. Zonation follows the northwest European classification system for regional biozones (Hoek, 1997a,b) as presented in Engels et al. (2022).

that the *n*-alkanes are well preserved in the sediments (Allen and Douglas, 1977) (Fig. 8b). The ACL curve shows stable values with a slight increase in average chain length across the Allerød/YD transition.

Compound-specific δD values are highest at the onset of the Allerød for all measured homologues and start to decrease prior to the Allerød/YD transition. δD_{C29} values decrease from an average value of −189‰ during the Allerød to an average value of −205‰ during the YD. δD_{C23} values decrease from −167‰ during the Allerød to −185‰ during the YD. This amounts to δD shifts of ca. −16‰ and −18‰, respectively. No change, or only very minor increases, are observed across the YD/Preboreal transition for both the short-chain alkanes (e.g. δD_{C23}) as well as the longer-chain alkanes (e.g. δD_{C27}, δD_{C31}) δD records.

GDGT-0, Crenarchaeol and total branched GDGT concentrations are relatively low during the Allerød (Fig. 9a), and show highest values during the first part of the YD. At ca. 12,240 cal a BP, GDGT concentrations decrease to stable and low values before increasing again at ca. 11,885 cal a BP. GDGT concentrations then remain stable across the YD/Preboreal transition. The GDGT-0/crenarchaeol ratio is well above 2 throughout the record and varies between 55 and 216 during the Allerød (Fig. 9b). BrGDGT-based MAF increases during the latter part of the Allerød biozone from 5.6 to 7.8 °C. The GDGT-0/crenarchaeol ratio abruptly decreases from >200 to around 10 across the Allerød/YD transition. MAF fluctuates around 6 °C during the first part of the YD, and decreases to ~4.5–5 °C at 12,270 cal a BP. MAF rapidly increases to 8 °C at ca. 11,865 cal a BP, after which brGDGT-inferred temperatures decline again to ca. 5 °C. The GDGT-0/crenarchaeol ratio increases abruptly to >300 at the onset of the Holocene. The MAF record remains relatively stable between ca. 5 and 6.5 °C across the YD/Preboreal transition.

3.4. Timing and duration of changes in biodiversity indicators

Onsets and duration of change have been determined for selected environmental and biodiversity parameters using piecewise linear regression, and results of the analyses are shown in Table 1a and b and Fig. 10. Where PLR was unable to identify reliable points of change (e.g. due to low numbers of samples), visually established change-points have been used to complete the data where possible. Proxies reflecting catchment-scale processes such as erosion rates (LOI) and hydrological conditions (δD_{C29} record) start to change at 12,845 and 12,840 cal a BP, respectively. These ages predate the start of the vegetation shift that defines the onset of the transition into the YD biozone at Lake Hämelsee, observed at 12,820 cal a BP (Fig. 10a–Engels et al., 2022), by a few decades. The GDGT-0/crenarchaeol ratio, an indicator of windiness in this lake (cf. Engels et al., 2022), is the first proxy to show change at the Allerød/YD transition, showing an onset of change dated to 12,885 cal a BP (Table 1a). The duration of the transitions for these environmental indicators at the Allerød/YD transition is 50–100 years. Onsets-of-change in the alpha diversity records for the pollen and *Pediastrum* datasets occur at 12,800 cal a BP, a few decades after the changes in the environmental records, and the diatom record shows a further decadal-scale delay in the onset of change, with the onset of change determined at 12,775 cal a BP. The alpha diversity record for the chironomid dataset does not show a unidirectional change across the Allerød-YD transition (Fig. 10b). It first shows increasing but highly variable alpha diversity after the Laacher See Eruption, followed by a gradual decrease in alpha diversity that starts several decades after the onset of the YD. Transitions in the pollen, *Pediastrum* and diatom alpha diversity records happen faster than transitions in the environmental records, with transitions taking 10–40 years (Fig. 10b). Changes in
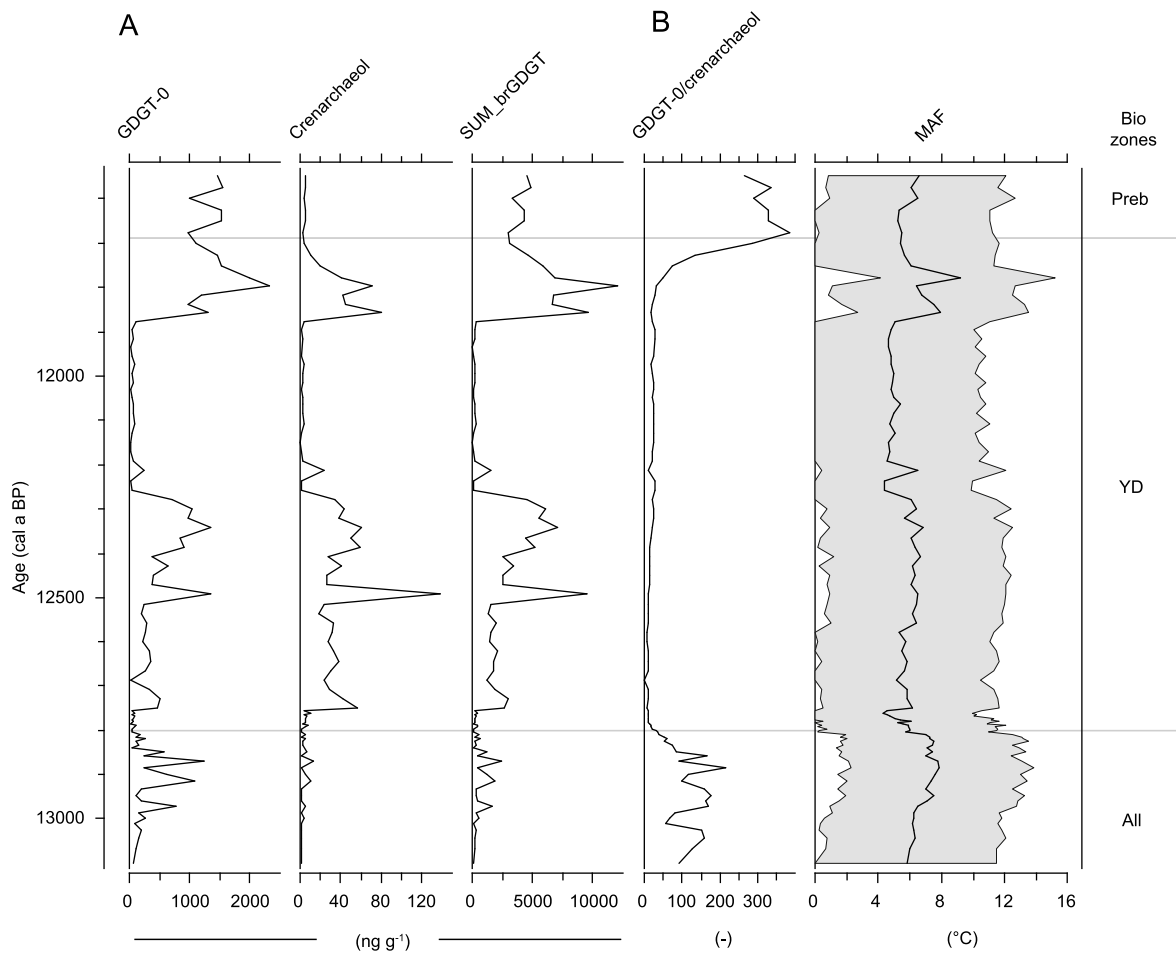
Fig. 9. GDGT record. (A) Concentrations of selected GDGTs (µg/g dry weight) and the total concentration of all branched GDGTs (sum brGDGT); (B) GDGT-/ crenarchaeol ratio and the mean temperature of months above freeing (MAF; °C) shown with a 95% uncertainty window. Note the individual x-axes used for each graph. Zonation follows the northwest European classification system for regional biozones (Hoek, 1997a,b) as presented in Engels et al. (2022).

chironomid compositional turnover start at 12,840 cal a BP, coinciding with the onset of change observed for some of the environmental parameters (LOI, δD). The onsets of change in the pollen compositional turnover record (12,805 cal a BP) and diatom compositional turnover record (12,780 cal a BP) show a decadal scale delay relative to the changes in the environmental records. Transition times vary strongly from 15 years for the diatom compositional turnover record to 185 years for the pollen compositional turnover record. The onset of change in the *Pediastrum* and pollen productivity records are only 5 years apart, at 12, 785 and 12,790 cal a BP, respectively, whereas the chironomid concentration record shows no clear signal at the Allerød/YD transition. The duration of changes in the pollen and *Pediastrum* productivity records are 30 and 40 years, respectively.

The YD/Preboreal transition is less clearly expressed in many of our records (Table 1b; Fig. 10c). The environmental indicators suggest onsets of change between 11,800 and 11,760 cal a BP, coinciding with the onset of the change toward the Preboreal as identified through pollen analysis (11,790 cal a BP; Engels et al., 2022). The duration of the observed changes varies between 100 and 125 years for the individual environmental records, which is slightly longer than the transition times observed for the Allerød/YD transition. Changes in alpha diversity are clearly identified in the pollen and chironomid records, showing onsets of change at 11,785 cal a BP and 11,725 cal a BP, respectively. Transitions for the pollen and chironomid records last 45–50 years, which is comparable to the transition times observed for the Allerød/YD transition. The diatom compositional turnover record shows changes starting in the late YD rather than at the YD/Preboreal transition (11,980 cal a

BP) and a long transition time of 300 years. The transition observed in the chironomid compositional turnover record coincides with the changes in the environmental records, starting at 11,800 cal a BP and lasting 50 years. Changes in the productivity records of *Pediastrum* and chironomids start after the changes in the environmental records (11, 725 and 11,800 cal a BP, respectively). The duration of the change in the *Pediastrum* flora at the onset of the Holocene is 50 years, whereas the chironomid record shows a transition time of 170 years.

4. Discussion

4.1. Palaeoenvironmental and palaeoclimatic development

4.1.1. Lake formation, Bølling and Older Dryas

The sandy lithology as well as the XRF results indicate a dynamic depositional environment with high detrital sediment in-flux during the oldest parts of our record. This is in line with inferences of the local presence of a fluvial environment characterised by permafrost conditions (Meinke, 1992), and situated within the wider cover sand region formed during the late Pleniglacial (Kasse, 2002). The pollen samples in the lowermost part of our record (pre- 14,200 cal a BP) did not yield high enough counts to reliably reconstruct regional or local vegetation patterns, but the chironomid assemblages were dominated by cold-indicating lacustrine taxa and suggest the presence of a nutrient-poor freshwater environment at the site. Abundant remains of semi-terrestrial chironomid taxa (e.g. *Pseudosmittia*; Fig. 7) were most likely transported into the lake from the surrounding floodplain during periods of flooding.
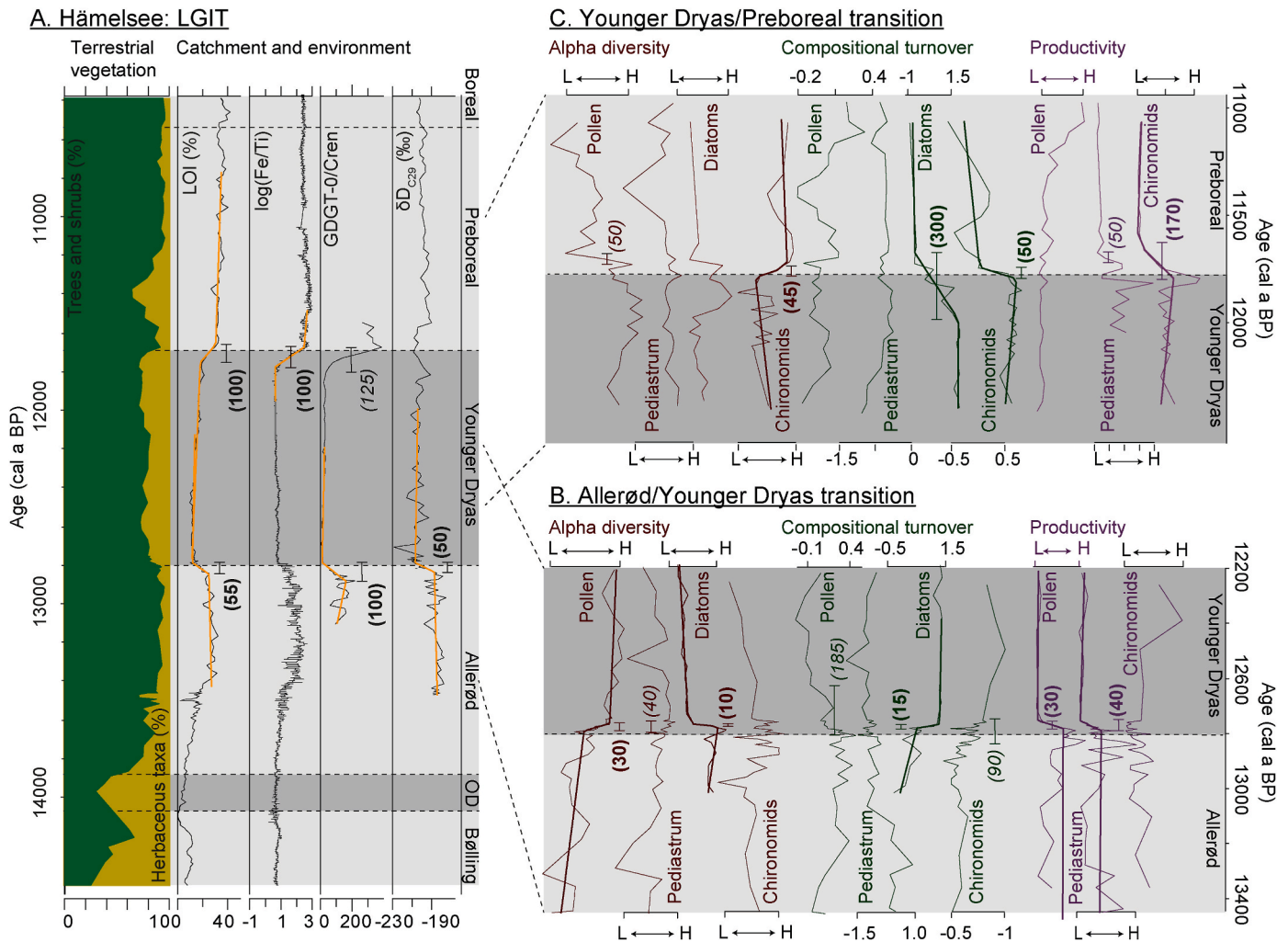
Fig. 10. Leads and lags in proxy records. (A) Summary records for the complete LGIT sequence at Lake Hämelsee with arboreal pollen percentages in darkgreen and non-arboreal pollen in yellow; (B) Detailed overview of the Allerød/YD transition; (C) Detailed overview of the YD/Preboreal transition. B and C show alpha diversity, compositional turnover and productivity curves for the palaeoecological proxies presented in this study. Linear overlays in A-C show the results of the Piecewise Linear Regression analysis, with whisker-symbols indicating the identified transition periods. Bracketed numbers (normal font and italic font) show the duration of the transition (as determined through PLR and visually, respectively) (see Table 1a and b); Dark shaded areas in each of the plots represent stadials; light shaded areas represent interstadials.

The first pollen samples that yielded counts that were high enough to reconstruct the vegetation at Hämelsee (14,200 cal a BP onward) show that the lacustrine deposits in this part of the record were deposited during the Bølling biozone. The pollen assemblages during the Bølling are initially characterised by high abundances of *Salix* (Fig. 4), similar to signals observed in pollen records from nearby sites in northeast (De Klerk, 2008) and central Germany (Litt and Stebich, 1999). The high abundances of *Salix* combined with the relatively high values of *Betula* during the Bølling suggest the presence of shrub vegetation (Litt et al., 2001). The finding of seeds of *Betula pubescens* in a previous core from Lake Hämelsee (Merkt and Müller, 1999) suggests some trees grew locally during the Bølling as well. A decrease in influx of terrestrial material into the lake is inferred from increasing LOI values and the disappearance of semi-terrestrial chironomid taxa, providing further evidence of landscape stabilisation during the Bølling. The chironomid assemblages indicate the presence of a permanent freshwater habitat without major inflow from rivers or streams from this time onward. *Microtendipes pedellus*-type and *Corynocera ambigua* are abundant during the Bølling and are typically considered as indicative of intermediate temperatures (Brooks et al., 2007), although cold-indicating taxa (e.g. *Tanytarsus lugens*-type) remain present during this phase. Similarly, the *Pediastrum* flora includes taxa associated with cool-temperate to cold

habitats (Turner et al., 2016). As C-IT values are variable and relatively low during the Bølling, the changes in vegetation composition and the increases in PAR and chironomid concentrations could reflect an increase in growing season length rather than an increase in summer temperatures (Wagner-Cremer and Lotter, 2011).

The increase in Poaceae during the Older Dryas suggests that the regional vegetation was more open and has been interpreted as representing the return of a steppe-tundra (Litt and Stebich, 1999; Litt et al., 2001; De Klerk, 2008). The concurrent increase in Si$_{clr}$ and the decreases observed in both the LOI and the Fe$_{clr}$ records could be the combined result of increased influx of clastic material with decreased in-lake organic production, respectively, as the landscape became more open.

The chironomid assemblages show high abundances of opportunistic taxa such as *M. pedellus*-type during the Older Dryas, when cold-indicator *S. rosenschoeldi*-type (Brooks et al., 2007) reaches maximum abundances. The *Pediastrum* assemblages consist of taxa typical for cool temperate to cold habitats (Turner et al., 2014, 2016) and the C-IT record shows relatively low reconstructed temperatures during the Older Dryas, in line with results elsewhere in central and western Europe (Heiri et al., 2014). Combined, the palaeoecological data suggests the existence of a nutrient-poor and cold lake environment during the Older Dryas.

Table 1a
Allerød/YD-transition.

Proxy	Parameter	Onset change (Cal a BP)	Duration	Author interpretation
Environmental indicators				
LOI	%-curve	12,845	55	
XRF	Log(Fe/Ti)	n/a	–	No clear signal
GDGT	GDGT-0/Cren	12,885	100	
δD	δD$_{C29}$	12,840	50	
Alpha diversity				
Pollen	Shannon of PS taxa	12,800	30	
Pediastrum	Shannon of all taxa	*12,800*	*40*	
Diatoms	Shannon of all taxa	12,775	10	
Chironomids	Shannon of all taxa	n/a	–	No clear signal
Compositional turnover				
Pollen	DCA axis 1	*12,805*	*185*	
Pediastrum	DCA axis 1	n/a	–	No clear signal
Diatoms	DCA axis 1	12,780	15	
Chironomids	DCA axis 1	*12,840*	*90*	
Productivity				
Pollen	PAR – arboreal pollen	12,785	30	
Pediastrum	PAR - all taxa	12,790	40	
Diatoms	Data not available	n/a	–	
Chironomids	concentrations	n/a	–	No clear signal

Onset and duration of change for selected environmental and biodiversity parameters, established using piecewise linear regression (normal font) or visually (italics). Ages provided in years cal a BP rounded to the nearest 5 year multiple.

Table 1b
YD/Preboreal-transition.

Proxy	Parameter	Onset change (Cal a BP)	Duration	Author interpretation
Environmental indicators				
LOI	%-curve	11,760	100	
XRF	Log(Fe/Ti)	11,775	100	
GDGT	GDGT-0/Cren	*11,800*	*125*	
δD	δD$_{C29}$	n/a	–	No clear signal
Alpha diversity				
Pollen	Shannon of PS taxa	*11,725*	*50*	
Pediastrum	Shannon of all taxa	n/a	–	No clear signal
Diatoms	Shannon of all taxa	n/a	–	Late-YD transition
Chironomids	Shannon of all taxa	11,785	45	
Compositional turnover				
Pollen	DCA axis 1	n/a	–	No clear signal
Pediastrum	DCA axis 1	n/a	–	No clear signal
Diatoms	DCA axis 1	11,980	300	Late-YD transition
Chironomids	DCA axis 1	11,800	50	
Productivity				
Pollen	PAR – arboreal pollen	n/a	–	No clear signal
Pediastrum	PAR - all taxa	*11,725*	*50*	
Diatoms	Data not available	n/a	–	
Chironomids	concentrations	11,800	170	

Onset and duration of change for selected environmental and biodiversity parameters, established using piecewise linear regression (normal font) or visually (italics). Ages provided in years cal a BP rounded to the nearest 5 year multiple.

4.1.2. Allerød

The subsequent increases in *Betula* and *Pinus* percentages during the Allerød reflect the transition to an increasingly denser birch- and birch-pine woodland with some restricted open habitats, similar to the development observed in other sites in central and western Europe (Brauer et al., 1999; Litt et al., 2001, 2003). The increasingly dense vegetation most likely led to soil stabilisation in the lake catchment, and the gradual decrease in Si$_{clr}$ indeed suggests a decrease in detrital sediment input (Fig. 3; Fig. 10). This is furthermore reflected in the diatom record, which shows a high percent-abundance of planktonic diatoms, indicating clear waters (Fig. 6). The preservation of varves, the high log(Fe/Ti) values and the high values of GDGT-0/crenarchaeol suggest phases of bottom-water anoxia, and the relatively high abundances of planktonic diatoms are also interpreted to suggest relatively strong lake water stratification during the Allerød. High summer temperatures (Fig. 7) were most likely the reason for the development of strong lake water stratification. This could have been further enhanced by low wind speeds as observed further south at Meerfelder Maar (Brauer et al., 2008).

The chironomid fauna present at Lake Hämelsee during the Allerød consists mostly of taxa that are typically associated with warm temperatures and the (sub-) littoral zones of lakes (Brooks et al., 2007), indicating the presence of a warm and relatively shallow lake during this time. Toward the end of the Allerød some taxa that are indicative of profundal habitats (e.g. *T. lugens-type, C. anthracinus*-type; Engels and Cwynar, 2011) increase in abundance. Some chironomid taxa that are abundant in this zone prefer raised nutrient levels (e.g. *Polypedilum nubeculosum*-type, *Cladotanytarsus mancus*-type; Brooks et al., 2007) and the relatively high abundance of planktonic diatom taxa in the late Allerød is also interpreted as reflecting relatively high nutrient levels (Liu et al., 2020).

The C-IT curve shows an abrupt increase to values of 14.5–15 °C at the start of the Allerød, which is followed by a slightly decreasing trend to values of ca. 13–14 °C during the second half of the Allerød, when the chironomid record shows increased abundances of cold-indicating *T. lugens*-type (Fig. 7). The increased abundances of *T. lugens*-type could either have been the result of actual cooling in the region of Lake Hämelsee, or the taxon could have inhabited the profundal zone of the former lake (c.f. Engels and Cwynar, 2011). The reconstructed temperatures for Lake Hämelsee are slightly lower than those observed for nearby Lake Hijkermeer (ca. 16 °C; Heiri et al., 2007) but higher than those derived for southern Sweden (ca. 11–12 °C; Muschitiello et al., 2015; Wohlfarth et al., 2017). The brGDGT-based MAF record shows an increasing trend between 13,100 and 12,810 cal a BP, which is in line with the C-IT record. Whilst many palaeoclimate records from Europe identify a number of centennial-scale climate oscillations during the Allerød (e.g. Lotter et al., 1992; Francis et al., 2021), our C-IT record does not show pronounced cooling in the latter part of the interstadial. This is in contrast with C-IT records from nearby sites such as Hijkermeer (Heiri et al., 2007) or the stable-isotope records from Greenland, which do show cooling during Greenland Interstadial GI-1b (Rasmussen et al., 2014). However, most *n*-alkane δD records of Lake Hämelsee (e.g. δD$_{C23}$, δD$_{C29}$) show a 120-year long episode of lower values during the late Allerød, indicating drier conditions and providing some evidence for the local registration of late-Allerød climate variability. We additionally do not observe a small-scale climate oscillation just prior to the onset of the YD as observed by Engels et al. (2016) at Lake Meerfelder Maar. Potentially, no ecological thresholds were crossed at Lake Hämelsee during these relatively low-amplitude and short climate oscillations, thus preventing their registration in our palaeoecological records. Alternatively, whereas climate oscillations such as GI-1b are clearly visible in C-IT records from sites in western Europe (e.g. UK, Francis et al., 2021; the Netherlands, Heiri et al., 2007), they might not be well-expressed in central and eastern European sites (c.f. Płóciennik et al., 2011), or they were expressed in climate parameters other than summer temperature.

4.1.3. Younger Dryas

The decrease in arboreal pollen and the increase in heliophilous taxa during the YD indicate that open habitats expanded, and vegetation

changed to a subarctic steppe tundra (Merkt and Müller, 1999; Litt et al., 2001). Aichner et al. (2018) attribute a shift to higher ACL values at Lake Trzechowskie to a change from a more tree-dominated to a more herbaceous and shrub-rich vegetation. Similarly, the shift towards higher ACL values at the Allerød/YD transition in the Hämelsee record (Fig. 8) could be the result of local changes in the vegetation (Fig. 4).

The lithology of our record changes from organic-rich varves to homogenous clay with low LOI values at the onset of the YD (Fig. 2; 3), which could have been the combined result of a decrease in temperature (Fig. 7), a return to shallow permafrost conditions (Hoek, 2001) and an increase in wind strength reducing stratification (Brauer et al., 2008). The latter is furthermore indicated by the presence of coarse sand visible in the microfacies, which possibly is of aeolian origin (c.f. Brauer et al., 2008). The concurrent increases in Si_{clr} and Ti_{clr} values (Fig. 3) are interpreted as reflecting increased input of terrestrial material into the lake system, either through in-wash or through aeolian deposition, whereas the decreases in e.g. the log(Ca/Ti) and log(Fe/Ti) records indicate a decrease in in-lake production and unstable lake conditions. The GDGT-0/crenarchaeol ratio is relatively low throughout the entire YD stadial, indicating relatively lower contributions of methanogens in the system (Blaga et al., 2009), similar to the changes observed for Lake Steisslingen in southern Germany (Weber et al., 2020). A decrease in methanogens could have been driven by increased amounts of lake water oxygen through increased mixing of the water column. The relative decrease in methanogens could also have been driven or strengthened by a loss of sediment organic matter, but the fact that changes in the GDGT records often predate those observed in the sedimentological indicators (e.g. LOI, XRF; Fig. 10a) suggests that methanogen production was primarily driven by lake water oxygen.

Chironomid taxon *M. pedellus*-type reaches maximum abundances during the Younger Dryas. This taxon typically thrives in a dynamic environment with minerogenic sediments (e.g. Engels et al., 2008). Additionally, chironomid taxa that are often associated with intermediate to cold environments (e.g. *M. insignilobus*-type, *S. rosenschoeldi*-type; Brooks et al., 2007) reach peak abundances during the Younger Dryas too. Similarly, *Pseudopediastrum kawraiskyi,* one of the most cold-tolerant species of the *Pseudopediastrum* genus (e.g. Komárek and Jankovská, 2001), reaches a maximum of >60% in the first half of the YD. The YD diatom assemblages are dominated by pioneer taxa such as fragilarioids (e.g. *S. pinnata, P. brevistriata*). These pioneer taxa have been characterised as well-adapted to unstable and often harsh conditions (Lotter and Bigler, 2000), and the assemblage shift toward fragilarioid taxa is therefore also interpreted as reflecting a shift toward cold water temperatures and low productivity levels with high turbidity.

The amplitude of YD-cooling (ca. 2 °C) in the C-IT record is similar to reconstructions for nearby sites in southern Sweden (Wohlfarth et al., 2017) and the Netherlands (Heiri et al., 2007), whereas sites further west (and therefore closer to the Atlantic) show a larger amplitude of change of ca. 4–5 °C (Heiri et al., 2014). The δD records of all *n*-alkane homologues show stable values across the YD, suggesting that no major changes in moisture source and pathways, or in evapotranspiration rates, occurred once a new state had been reached following the Allerød/YD-transition. Whilst the long-chain *n*-alkane δD records ($δD_{C27}$-$δD_{C31}$) at both Hämelsee and Meerfelder Maar show a decrease of ca. 10–15‰ across the Allerød/YD transition, the $δD_{C27}$ record from Hässeldala Port shows only a decrease of ca. 5‰ (Muschitiello et al., 2015). This difference in amplitude is thought to have resulted from increased freshwater forcing from the Fennoscandian Ice Sheet to the Nordic Seas, which would have led to spatially divergent hydrological changes across the European continent (Muschitiello et al., 2015; Wohlfarth et al., 2017).

The MAF record shows an amplitude of cooling (ca. 2 °C) at the onset of the YD similar to the cooling observed in the C-IT record. MAF temperatures of ca. 6 °C are observed during the first part of the YD, when e. g. cold-indicator *Pediastrum* taxon *Pp. kawraiskyi* shows its highest

abundances of the entire record. The MAF record shows a further reduction of reconstructed temperatures in the second half of the YD, predating the occurrence of *Empetrum* (ca. 12,180 cal a BP) by ca. 60 years, indicating the establishment of a more continental climate, consistent with increased dune formation in this region (Merkt and Müller, 1999). However, the Si_{clr} record does not show an increase during the second half of the YD, and the LOI record shows a minor increase (Fig. 3) at this time. Interestingly, a colder second phase of the YD is not consistently recognized in other GDGT-based temperature records. For example, it is not recorded by isoGDGTs in Lake Lucerne (Blaga et al., 2013), but brGDGTs in Lake Steisslingen (southern Germany) do show a temperate decrease during the second half of the YD (Weber et al., 2020). Notably, the C-IT record shows a slight increase from around 12,100 cal a BP onward (Fig. 7), which is in line with results by Müller et al. (2021) who also show a slight increase in summer temperatures inferred from chironomids during the second half of the YD for Lake Gościąż, but which contrasts the cooling observed in the MAF reconstruction. Additionally, whereas the MAF record shows a relatively abrupt increase in temperatures around 11,900 cal a BP., the C-IT record shows a slight decrease in temperatures around this time (Fig. 7; Fig. 9). The offset between the GDGT and the chironomid records at Lake Hämelsee may be introduced by the fact that the proxies record temperatures during a different part of the year. Specifically, the brGDGTs reflect the mean temperature for months above freezing (Martinez-Sosa et al., 2021), which makes this indicator more sensitive to changes in winter temperatures than chironomids that mostly record summer temperatures.

The timing of the increase in *Empetrum* in the second half of the YD, just before the occurrence of the Vedde Ash (dated 12,065 ± 50 cal a BP, Lohne et al., 2014), compares well to results at, e.g., nearby Kostverlorenveen (Davies et al., 2005) as well as elsewhere in Europe (Lane et al., 2013). The concentrations of all *n*-alkane homologues increase in the second half of the YD. We suggest that the increased concentrations of *n*-alkanes in the Hämelsee record were not the result of a shift in climate. Instead, increased alkane production by the extant vegetation, better preservation, or more direct transport of alkanes from the catchment into the lake might explain the increase in *n*-alkane concentrations.

4.1.4. Preboreal

Whilst some birch trees were already present in the region in the late YD (Hoek, 2001), the abrupt increase in *Betula* at the onset of the Holocene indicates the development of dense boreal birch-woodland in the Hämelsee region. A short-lived increase in Poaceae represents the drier and more continental Rammelbeek phase (11,550 and 11,190 cal a BP; Hoek and Bos, 2007) and is followed by a phase of high percent-abundances of AP, suggesting the occurrence of a closed-canopy forest at Hämelsee (Merkt and Müller, 1999). Total *n*-alkane concentrations decrease at the onset of the Preboreal (Fig. 8). As pollen percentages and PAR of broad-leafed vegetation increase at this point (Fig. 4), we suggest that the decrease in *n*-alkane concentrations is the result of decreased transport to the lake rather than of a lower alkane-production by the extant vegetation. This is in line with the decrease in Si_{clr} and Ti_{clr} which suggests a decrease in erosional activity.

All cold-indicating chironomid taxa decline in abundance at the onset of the Preboreal and are replaced by warm stenothermic taxa. Similarly, cold-indicating *Pediastrum* taxa completely disappear from the assemblage at the onset of the Holocene and are replaced by thermophilic taxa. The chironomid fauna, the *Pediastrum* flora and the diatom flora all indicate the existence of a relatively nutrient-rich lake during the Preboreal.

The lithology shows a return to laminated sediments, indicating deposition under oxygen-poor conditions (e.g. high log(Fe/Ti) and log (Ca/Ti) values). This is in line with the abrupt increase in the GDGT-0/ crenarchaeol record, which indicates strong seasonal lake stratification and reduced windiness. The GDGT-0/crenarchaeol record for Lake

Steisslingen shows a similar return to very high values at the onset of the Holocene (Weber et al., 2020). Furthermore, the abrupt switch from a benthic- to a planktonic-dominated diatom assemblage (Fig. 6) likely reflects the re-establishment of anoxic conditions at the lake bottom and illustrates the sensitive response of the aquatic system to climate warming.

C-ITs increase abruptly from ca. 12 °C to values of 14–17 °C at the onset of the Preboreal. Both the absolute reconstructed values as well as the amplitude of change across the YD/Preboreal transition compare well to a C-IT record for Lake Hijkermeer (Heiri et al., 2007). Chironomid-based temperature inferences for the Preboreal derived for sites from the British Isles are similar to those at Hämelsee, whereas Preboreal temperatures for southern Sweden are slightly lower than those at Hämelsee (Wohlfarth et al., 2017, 2018). This indicates that the east-west gradient in summer temperatures during the Preboreal was less steep compared to the gradient during the YD. The brGDGT-derived MAF record shows an abrupt increase of ca. 4 °C at 11,900 cal a BP, more than 100 years before the onset of the Preboreal (11,790 cal a BP) before decreasing to values of ca. 7–8 °C during the early part of the Preboreal. Minor increases in δD values are observed across the YD/Preboreal transition, in line with results at Meerfelder Maar (Rach et al., 2014). Results from southern Sweden do not show a minor increase in δD values at this time, potentially reflecting a spatially heterogeneous hydroclimatic development around the onset of the Preboreal (Muschitiello et al., 2015).

4.2. Differences in timing and duration of biodiversity response to external forcing

4.2.1. Allerød/Younger Dryas transition

Environmental indicators are the first to show changes in the Hämelsee record (Table 1a and b). These indicators might be able to respond quickly to early climate change as they are directly impacted by ambient temperatures or changes in weather conditions. For instance, higher allochthonous sediment influx into central European lakes is often directly linked to increases in storminess (Brauer et al., 2008; Martin-Puertas et al., 2012). The decadal-scale differences in the identified onsets-of-change in our environmental indicators might be the result of differences in proxy-sensitivity, of sampling resolution, or they might reflect differences between the onset of change in individual components of the climate system. Whilst we would expect that on a decadal to centennial scale climate parameters such as winter and summer temperatures, precipitation or storminess change synchronously, it might be the case that, on shorter time intervals, certain parameters change more independently. The delayed start of changes in δD at 12,840 cal a BP (reflecting changes in the hydroclimate) relative to the changes observed in, e.g., the GDGT-0/crenarchaeol record (reflecting changes in lake stratification, potentially driven by changes in windiness) could indeed suggest that certain aspects of the climate system acted independently.

Several of the palaeoecological records show onsets of change that postdate the changes observed in the environmental records by a few decades. The diatom flora in particular shows a delayed response in decrease of alpha diversity as well as in compositional turnover record relative to the onsets of changes in the environmental records. Similarly, the *Pediastrum* productivity record shows a relatively late onset of change. The duration of the changes in the *Pediastrum* and diatom records is, however, very short (10–40 years) suggesting that the assemblages showed resilience to external pressure before reaching a critical tipping point, after which they quickly transitioned to a new community composition. The chironomid alpha diversity record shows an increase in diversity during the late Allerød and into the YD. Potentially, the weakening of lake water stratification provided a larger and more diverse habitat for these organisms before more direct effects of cooling started to impact the chironomid fauna (Engels et al., 2020). The combined evidence at the Allerød/YD transition suggests that biodiversity

records responded with a decadal-scale delay to changes in the physical environment, and that for some indicator groups changes in lake water stratification played an important role. Similarly, a high-resolution multi-proxy study from Poland suggested that lake internal processes including stratification and mixing duration were important drivers of the biotic composition of the lake across the Allerød/YD transition (Słowiński et al., 2017).

The duration of the changes observed in the environmental parameters was 50–100 years, which is longer than the duration of changes in the alpha diversity records (10–40 years) and most of the other biodiversity indicators (Table 1a and b); in particular, the diatom record shows very abrupt changes in the order of 10–15 years. Similarly fast transition times are in line with results from other lakes in central and northwest Europe. For instance, Słowiński et al. (2017) observed a transition in the Lake Trzechowskie (Poland) diatom record that lasted 55 years. Similarly, Birks et al. (2000) observed changes in aquatic proxies at Kråkenes (Norway) across the Allerød/YD transition that lasted several decades. Birks et al. (2000) attributed this multi-decadal transition to a combination of changes in air and water temperatures, as well as the impact of these changes on the lake catchment. At Kråkenes, increased solifluction and soil in-wash due to climate cooling led to increased input of silt and other terrestrial material into the lake ecosystem, which ultimately led to increased turbidity and the destruction of the aquatic macrophyte vegetation and of the habitats these plants provided, thus indirectly impacting the aquatic flora and fauna. It is likely that at Hämelsee the aquatic proxies were also impacted by both direct and indirect effects of climate change, as we, for example, observe changes in sediment influx from the catchment at the onset of the YD.

Changes in compositional turnover for the chironomid and pollen records at the onset of the YD take 90 and 185 years to reach a new state, respectively, which is much longer than the duration of changes observed for the other parameters. The duration of the vegetation response might have been influenced by a combination of factors including the longevity of vegetation present during the late Allerød, the shading effects of moribund vegetation on seedlings, and soil properties including nutrient availability and moisture retention. A relatively long period of vegetation response to LGIT climate cooling is in line with observations elsewhere that show that transitions in pollen assemblages can last from several decades (Litt et al., 2001) up to 100–200 years (Goslar et al., 1995), but contrasts with results from Meerfelder Maar (MFM), where Brauer et al. (1999) showed that vegetation changes occurred within 20 years at the beginning of the Younger Dryas. The difference between MFM and our Hämelsee record might be due to the exceptional situation of MFM situated deep in a Maar crater, with crater walls attenuating wind stress over the lake surface (Brauer et al., 2008). The chironomid fauna at Lake Hämelsee might have been responding to a number of direct (e.g. climate) and indirect (e.g. oxygen availability, habitat availability) drivers at the Allerød/YD transition, which could have led to a relatively long period of change. Similarly, a 140–180 year long transition is observed for the high-resolution chironomid record of Lake Gościąż (Müller et al., 2021).

4.2.2. Younger Dryas/Preboreal-transition

The YD/Preboreal transition is less clearly expressed in many of our Hämelsee proxy-records (Fig. 10b). This is perhaps somewhat surprising as typically this transition is clearly visible as an abrupt shift in pollen- and other proxy-records e.g. from lakes in northwest Europe. For instance, Birks et al. (2000) observed that all proxy-indicators analysed in the Kråkenes record showed large and rapid changes in response to the temperature rise characterising the YD/Preboreal transition.

The environmental indicators in the Lake Hämelsee record suggest onsets of change between 11,800 and 11,760 cal a BP, coinciding with or slightly later than the onset of the change toward the Preboreal as identified through pollen analysis (11,790 cal a BP; Engels et al., 2022). The chironomid fauna at Hämelsee shows contemporary onsets of

changes in its diversity, compositional turnover and productivity records (11,800–11,785 cal a BP). This result is in line with results from Kråkenes where chironomids were also observed as responding rapidly to environmental and climatic changes related to the onset of the Holocene (Birks et al., 2000). The increase in chironomid alpha diversity at the onset of the Holocene is in line with results by Engels et al. (2020) who showed a positive relationship between chironomid diversity and summer temperature in both space and time. Similar to the delay observed at the Allerød/YD transition, the pollen alpha diversity record shows an onset of change at 11,725 cal a BP, several decades after most other records started to change. This relatively late onset might again have been due to a combination of factors including nutrient availability, soil moisture conditions, or the time it takes for the expansion of tree birch to ultimately outshade or otherwise outcompete the herbaceous and heliophylic taxa present in the lake catchment. The trend in the diatom alpha diversity curve is of note; it shows a non-linear change with maximum diversity occurring well before the YD/Preboreal transition. This maximum could reflect an early onset of change and a period where the taxa that were dominating the diatom assemblages during the YD are still present with the taxa typical for the Preboreal increasing in abundance. Once the Preboreal was fully established, diatom preservation is very poor (Fig. 6). Higher water temperature and pH, as well as increased invertebrate activity, can promote diatom silica dissolution in freshwater lakes (Ryves et al., 2013). Whereas the *Pediastrum* record does not show a change in compositional turnover across the YD/Preboreal transition, both the chironomid and *Pediastrum* records show a decrease in productivity at this time. This decrease is potentially due to changes in lake water stratification strength or in mixing duration, which would have impacted aquatic habitat availability (cf. Słowiński et al., 2017).

The duration of the observed changes varies between 100 and 125 years for the individual environmental records, which is longer than the transition times observed for the Allerød/YD transition. This relatively long response time could be related to the time it took for vegetation to develop and protect soil against erosion. The alpha diversity and compositional turnover records show transitions that lasted 45–50 years, which is in line with transition times during the Allerød/YD transition as well as to the transition as observed elsewhere (e.g. Birks et al., 2000). The productivity records were slower to change, as they show a response time in the order of 50 (*Pediastrum*) and 170 (chironomids) years. The diatom compositional turnover record shows an even longer transition period of 300 years. These responses could have been influenced directly by relatively fast processes such as climate change, as well as by more delayed and indirect drivers such as nutrient influx from the catchment, which could have changed more gradually as a result of ongoing establishment of birch woodland.

5. Concluding remarks

The LGIT sediment record from Lake Hämelsee combines a robust chronological framework with a high sedimentation rate, allowing for a detailed reconstruction of environmental and ecosystem change across key climatic transitions. Using a range of proxy-indicators we show the dynamic palaeoenvironmental development from the Bølling to the early Holocene (ca. 14,500–10,500 cal a BP), and we reconstruct changes in summer and mean annual air temperatures, hydroclimate and windiness, as well as their effects on the aquatic environment at Lake Hämelsee. We show that the development of the terrestrial environment was typical of Lateglacial sites in northwest Europe, with the establishment of birch and birch-pine woodland during the Bølling/Allerød interstadial, a return to a subarctic steppe tundra during the YD and renewed afforestation during the Preboreal. The aquatic ecosystem supported flora and fauna that were characterised by warm-indicating taxa that are typically associated with higher nutrient levels during the Bølling/Allerød interstadial, with the establishment of lake water stratification and bottom water anoxia in the late Allerød. Most of these

taxa decreased in abundance or disappeared during the YD and were replaced by cold-indicating flora and fauna typically associated with lower nutrient levels and a higher disturbance regime. The climatic and environmental changes during the YD prevented extended lake water stratification. At the onset of the Holocene a return to warm conditions with higher nutrient levels and more pronounced lake water stratification was observed.

Ecosystem response to LGIT climate change was complex, and we observe decadal-scale differences in timing and duration of individual proxy responses to LGIT climate change. Specifically, we observe that onsets of changes in biodiversity parameters lag environmental indicators by a few decades, particularly at the Allerød/YD transition. Most biodiversity records showed transitions that lasted 10–50 years, with slightly longer transitions recorded for the environmental parameters. The longer transition times observed for some of the biodiversity parameters could be the result of combined effects of both direct (e.g. climate) and indirect drivers (e.g. nutrient availability, oxygen concentrations) of ecosystem change, with a particularly important role for lake water stratification. More high-resolution, well-dated palaeoecological records are needed to provide crucial information on timing and trends in biodiversity and the effects of direct and indirect drivers on community composition. Such information will be of key importance for effective conservation management and ecological restoration of heavily impacted freshwater ecosystems under current global warming.

Data availability

The proxy-data presented in this paper has been made publicly available through the PANGAEA data repository as Engels S, Lane CS, Hoek WZ, Baneschi I, Bouwman A, Brogan E, Bronk Ramsey C, Collins JA, de Bruijn R, Haliuc A, Heiri O, Hubay K, Jones G, Jones V, Laug A, Merkt J, Muschitiello F, Muller M, Peters T, Peterse F, Pueschel A, Staff RA, ter Schure A, van den Bos V, Wagner-Cremer F (2024): Lake Hämelsee: Lateglacial sedimentological, palaeoecological and geochemical data. PANGAEA, https://doi.org/10.1594/PANGAEA.964375. Individual datasets can be accessed as follows:

- Engels et al. (2024) Loss on ignition in sediment core Haem13 from lake Hämelsee. https://doi.org/10.1594/PANGAEA.964380
- Engels et al. (2024) Selected major and minor elements and element ratios in sediment core Haem13 from lake Hämelsee. https://doi.org/10.1594/PANGAEA.964382
- Engels et al. (2024) Pediastrum taxa as percentage of the total Pediastrum count sum in sediment core Haem13 from lake Hämelsee. https://doi.org/10.1594/PANGAEA.964399
- Engels et al. (2024) Individual valve counts of diatoms in sediment core Haem13 from lake Hämelsee. https://doi.org/10.1594/PANGAEA.964521
- Engels et al. (2024) Chironomidae whole or half head capsules counts in sediment core Haem13 from lake Hämelsee. https://doi.org/10.1594/PANGAEA.964523
- Engels et al. (2024) Dry mass concentrations of individual n-alkanes in sediment core Haem13 from lake Hämelsee. https://doi.org/10.1594/PANGAEA.964524
- Engels et al. (2024) δDeuterium measurements of selected n-alkanes (corrected to the VSMOW scale) in sediment core Haem13 from lake Hämelsee. https://doi.org/10.1594/PANGAEA.964525
- Engels et al. (2024) GDGTs in sediment core Haem13 from lake Hämelsee. https://doi.org/10.1594/PANGAEA.964381

The pollen data generated for the Haem13 cores (originally presented in Engels et al. (2022)) are available in the PANGAEA repository (https://doi.org/10.1594/PANGAEA.939693). The R code used for PLR calculations can be found in the Supplementary Information.

Author contributions

Conceptualisation, methodology and funding acquisition: SE, CSL, DS, WZH; Investigation: SE, CSL, DS, WZH, IB, ABo, ABr, EB, JC, RdB, AH, KH, GJ, AL, FM, MM, TP, FP, AP, AtS, FT, VvdB; Resources: WZH, CBR, OH, JM, RS, FWC; Writing – original draft: SE; Writing – review and editing: all co-authors.

Declaration of competing interest

The authors declare that they have no known competing financial interests or personal relationships that could have appeared to influence the work reported in this paper.

Acknowledgements

Appendix A. Supplementary data

Supplementary data to this article can be found online at https://doi.org/10.1016/j.quascirev.2024.108634.

References

Aichner, B., Ott, F., Słowiński, M., Noryśkiewicz, A.M., Brauer, A., Sachse, D., 2018. Leaf wax n-alkane distributions record ecological changes during the Younger Dryas at Trzechowskie paleolake (northern Poland) without temporal delay. Clim. Past 14, 1607–1624.

Allen, J., Douglas, A.G., 1977. Variations in the content and distribution of n-alkanes in a series of carboniferous vitrinites and sporinites of bituminous rank. Geochem. Cosmochim. Acta 41, 1223–1230.

Bechtel, A., Smittenberg, R.H., Bernasconi, S.M., Schubert, C.J., 2010. Distribution of branched and isoprenoid tetraether lipids in an oligotrophic and a eutrophic Swiss lake: insights into sources and GDGT-based proxies. Org. Geochem. 41, 822–832.

Birks, H.H., Birks, H.J.B., 2013. Vegetation responses to late-glacial climate changes in western Norway. Preslia 85, 215–237.

Birks, H.H., Battarbee, R.W., Birks, H.J.B., project contributors, 2000. The development of the aquatic ecosystem at Kråkenes Lake, western Norway, during the late-glacial and early-Holocene – a synthesis. J. Paleolimnol. 23, 91–114.

Birks, H.J.B., Line, J.M., Juggins, S., Stevenson, A.C., ter Braak, C.J.F., 1990. Diatoms and pH reconstruction. Philos. Trans. R. Soc. London, Ser. A B 327, 263–278.

Birks, H.J.B., Felde, V.A., Seddon, A.W.R., 2016a. Biodiversity trends within the Holocene. Holocene 26, 994–1001.

Birks, H.J.B., Felde, V.A., Bjune, A.E., Grytnes, J.-A., Seppä, H., Giesecke, T., 2016b. Does pollen-assemblage richness reflect floristic richness? A review of recent developments and future challenges. Rev. Palaeobot. Palynol. 228, 1–25.

Blaga, C.I., Reichart, G.-J., Heiri, O., Sinninghe Damsté, J.S., 2009. Tetraether membrane lipid distributions in water-column particulate organic matter and sediments: a study of 47 European lakes along a north–south transect. J. Paleolimnol. 41, 523–540.

Blaga, C.I., Reichart, G.-J., Lotter, A.F., Anselmetti, F.S., Sinninghe Damsté, J.S., 2013. A TEX86 lake record suggests simultaneous shifts in temperature and Greenland during the last deglaciation. Geophys. Res. Lett. 40, 948–953.

Bos, J.A.A., van Geel, B., van der Plicht, J., Bohncke, S.J.P., 2007. Preboreal climate oscillations in Europe: Wiggle-match dating and synthesis of Dutch high-resolution multi-proxy records. Quat. Sci. Rev. 26, 1927–1950.

Brauer, A., Endres, C., Günter, C., Litt, T., Stebich, M., Negendank, J.F.W., 1999. High resolution sediment and vegetation responses to Younger Dryas climate change in varved lake sediments from Meerfelder Maar, Germany. Quat. Sci. Rev. 18, 321–329.

Brauer, A., Haug, G.H., Dulski, P., Sigman, D.M., Negendank, J.W.F., 2008. An abrupt wind shift in western Europe at the onset of the Younger Dryas cold period. Nat. Geosci. 1, 520–523.

Bronk Ramsey, C., 2009. Bayesian analysis of radiocarbon dates. Radiocarbon 51, 337–360.

Brooks, S.J., Langdon, P.G., Heiri, O., 2007. The identification and use of Palaearctic Chironomidae Larvae in palaeoecology. In: Quaternary Research Association Technical Guide No. 10. Quaternary Research Association, London.

Brooks, S.J., Langdon, P.G., 2014. Summer temperature gradients in northwest Europe during the Lateglacial to early Holocene transition (15–8 ka BP) inferred from chironomid assemblages. Quat. Int. 341, 80–90.

Camburn, K., Charles, D., 2000. Diatoms of low-alkalinity lakes in the Northeastern United States. Academy of Natural Sciences of Philadelphia, p. 152.

Colombaroli, D., Tinner, W., 2013. Determining the long-term changes in biodiversity and provisioning services along a transect from Central Europe to the Mediterranean. Holocene 23, 1625–1634.

Davies, S.M., Hoek, W.Z., Bohncke, S.J.P., Lowe, J.J., Pyne O'Donnell, S., Turney, C.S.M., 2005. Detection of Lateglacial distal tephra layers in The Netherlands. Boreas 34, 123–135.

De Jonge, C., Hopmans, E.C., Zell, C.I., Kim, J.H., Schouten, S., Sinninghe Damsté, J.S., 2014. Occurrence and abundance of 6-methyl branched glycerol dialkyl glycerol tetraethers in soils: implications for palaeoclimate reconstruction. Geochem. Cosmochim. Acta 141, 97–112.

De Klerk, P., 2008. Patterns in vegetation and sedimentation during theWeichselian Lateglacial in north-eastern Germany. J. Biogeogr. 35, 1308–1322.

Dearing Crampton-Flood, E., Tierney, J.E., Peterse, F., Kirkels, F.M.S.A., Sinninghe Damsté, J.S., 2020. BayMBT: a Bayesian calibration model for branched glycerol dialkyl glycerol tetraethers in soils and peats. Geochem. Cosmochim. Acta 268, 142–159.

Dudgeon, D., Arthinton, A.H., Gessner, M.O., Kawabata, Z.-I., Knowler, D.J., Lévêque, C., Naiman, R.J., Prieur-Richard, A.-H., Soto, D., Stiassny, M.L.J., Sullivan, C.A., 2006. Freshwater biodiversity: importance, threats, status and conservation challenges. Biol. Rev. 81, 163–182.

Engels, S., Cwynar, L.C., 2011. Changes in fossil chironomid remains along a depth gradient: evidence for common faunal thresholds within lakes. Hydrobiologia 665, 15–38.

Engels, S., Bohncke, S.J.P., Bos, J.A.A., Brooks, S.J., Heiri, O., Helmens, K.F., 2008. Chironomid-based palaeotemperature estimates for northeast Finland during oxygen isotope stage 3. J. Paleolimnol. 40, 49–61.

Engels, S., Helmens, K.F., Väliranta, M., Brooks, S.J., Birks, H.J.B., 2010. Early Weichselian (MIS 5d and 5c) temperatures and environmental changes in northern Fennoscandia as recorded by chironomids and macroremains at Sokli, northeast Finland. Boreas 39, 689–704.

Engels, S., Brauer, A., Buddelmeijer, N., Martin-Puertas, C., Rach, O., Sachse, D., van Geel, B., 2016. Subdecadal-scale vegetation responses to a previously unknown late-Allerød climate fluctuation and Younger Dryas cooling at Lake Meerfelder Maar (Germany). J. Quat. Sci. 31, 741–752.

Engels, S., Medeiros, A.S., Axford, Y., Brooks, S.J., Heiri, O., Luoto, T.P., Nazarova, L., Porinchu, D.F., Quinlan, R., Self, A.E., 2020. Temperature change as a driver of spatial patterns and long-term trends in chironomid (Insecta: Diptera) diversity. Global Change Biol. 26, 1155–1169.

Engels, S., Lane, C.S., Haliuc, A., Hoek, W.Z., Muschitiello, F., Baneschi, I., Bouwman, A., Bronk Ramsey, C., Collins, J., de Bruijn, R., Heiri, O., Hubay, K., Jones, G., Laug, A., Merkt, J., Müller, M., Peters, T., Peterse, F., Staff, R., ter Schure, A., Turner, F., van den Bos, V., Wagner-Cremer, F., 2022. Synchronous vegetation response to the last glacial-interglacial transition in northwest Europe. Commun. Earth Environ. 3, 130.

Faegri, K., Iversen, J., 1989. Textbook of Pollen Analysis. Wiley, Chichester.

Ficken, K.J., Li, B., Swain, D.L., Eglinton, G., 2000. An n-alkane proxy for the sedimentary input of submerged/floating freshwater aquatic macrophytes. Org. Geochem. 31, 745–749.

Francis, C.P., Candy, I., Engels, S., Matthews, I., Palmer, A.P., Timms, R.G.O., Jordan, A.-L., 2021. The magnitude of the lateglacial interstadial cooling events at Crudale Meadow, Orkney (UK). J. Quat. Sci. 36, 325–338.

Goslar, T., Arnold, M., Bard, E., Kuc, T., Pazdur, M.F., Ralska-Jasiewiczowa, M., Różański, K., Tisnérat, N., Walanus, A., Wicik, B., Wiqkowski, K., 1995. High concentration of atmospheric 14C during the Younger Dryas cold episode. Nature 377, 414–417.

Gregory-Eaves, I., Beisner, B.E., 2011. Palaeolimnological insights for biodiversity science: an emerging field. Freshw. Biol. 56, 2653–2661.

Guiry, M.D., Guiry, G.M., 2024. AlgaeBase. World-wide Electronic Publication. National University of Ireland, Galway. https://www.algaebase.org.

Heiri, O., Lotter, A.F., 2001. Effect of low count sums on quantitative environmental reconstructions: an example using subfossil chironomids. J. Paleolimnol. 26, 343–350.

Heiri, O., Lotter, A.F., Lemcke, G., 2001. Loss on ignition as a method for estimating organic and carbonate content in sediments: reproducibility and comparability of results. J. Paleolimnol. 25, 101–110.

Heiri, O., Cremer, H., Engels, S., Hoek, W., Peeters, W., Lotter, A.F., 2007. Late-Glacial summer temperatures in the Northwest European lowlands: a new chironomid record from Hijkermeer, The Netherlands. Quat. Sci. Rev. 26, 2420–2437.

Heiri, O., Brooks, S.J., Birks, H.J.B., Lotter, A.F., 2011. A 274-lake calibration data-set and inference model for chironomid-based summer air temperature reconstruction in Europe. Quat. Sci. Rev. 30, 3445–3456.

Heiri, O., Brooks, S.J., Renssen, H., Bedford, A., Hazekamp, M., Ilyashuk, B., Jeffers, E.S., Lang, B., Kirilova, E., Kuiper, S., Millet, M., Samartin, S., Toth, M., Verbruggen, F., Watson, J.E., van Asch, N., Lammertsma, E., Amon, L., Birks, H.H., Birks, H.J.B.,

Mortensen, M.F., Hoek, W.Z., Magyari, E., Muñoz Sobrino, C., Seppä, H., Tinner, W., Tonkov, S., Veski, S., Lotter, A.F., 2014. Validation of climate model-inferred regional temperature change for late-glacial Europe. Nat. Commun. 5, 4914.

Hoek, W.Z., 1997a. Atlas to Palaeogeography of Lateglacial Vegetations. Maps of Lateglacial and Early Holocene Landscape and Vegetation in The Netherlands, with an Extensive Review of Available Palynological Data. Nederlandse Geografische Studies. ISSN 0169-4839, 231.

Hoek, W.Z., 1997b. Late-Glacial and early Holocene climatic events and chronology of vegetation development in The Netherlands. Veg. Hist. Archaeobotany 6, 197–213.

Hoek, W.Z., 2001. Vegetation response to the ~14.7 and ~11.5 ka cal. BP climate transitions: is vegetation lagging climate? Global Planet. Change 30, 103–115.

Hoek, W.Z., Bos, J.A.A., 2007. Early Holocene climate oscillations—causes and consequences. Quat. Sci. Rev. 26, 1901–1906.

Hopmans, E.C., Schouten, S., Damsté, J.S.S., 2016. The effect of improved chromatography on GDGT-based palaeoproxies. Org. Geochem. 93, 1–6.

IPCC (Intergovernmental Panel on Climate Change), 2021. Climate Change 2021: the Physical Science Basis. Contribution of Working Group I to the Sixth Assessment Report. Cambridge University Press, Cambridge, United Kingdom and New York, NY, USA.

Jansen, B., Haussmann, N.S., Tonneijck, F.H., Verstraten, J.M., de Voogt, P., 2008. Characteristic straight-chain lipid ratios as a quick method to assess past forest-páramo transitions in the Ecuadorian Andes. Palaeogeogr. Palaeoclimatol. Palaeoecol. 262, 129–139.

Jones, G., Lane, C.S., Brauer, A., Davies, S.M., De Bruijn, R., Engels, S., Haliuc, A., Hoek, W.Z., Merkt, J., Sachse, D., Turner, F., Wagner-Cremer, F., 2018. The Lateglacial to early Holocene tephrochronological record from Lake Hämelsee, Germany: a key site within the European tephra framework. Boreas 47, 28–40.

Juggins, S., 2007. C2 User Guide. Software for Ecological and Palaeoecological Data Analysis and Visualisation. University of Newcastle, Newcastle upon Tyne.

Juggins, S., 2017. Rioja: analysis of quaternary science data. R package version (0.9–21). http://cran.r-project.org/package=rioja.

Kasse, C., 2002. Sandy aeolian deposits and environments and their relation to climate during the Last Glacial Maximum and Lateglacial in northwest and central Europe. Prog. Phys. Geogr. Earth Environ. 26, 507–532.

Komárek, J., Jankovská, V., 2001. Review of the green algal genus *Pediastrum*; implication for pollen-analytical research. Bibl. Phycol. 108, 1–127.

Krammer, K., Lange-Bertalot, H., 1986. Süßwasserflora von Mitteleuropa. In: Ettl, H., Gerloff, J., Heynig, H., Mollenhauer, D. (Eds.), Bacillariophyceae. Naviculaceae. G. Fischer, Stuttgart. New York, 2/1, 876 pp.; Bacillariaceae, Epithemiaceae, Surirellaceae, 2/2, 596 pp.; Centrales, Fragilariaceae, Eunotiaceae, 2/3, 576 pp.; Achnanthaceae, 2/4, 437.

Lane, C.S., Brauer, A., Blockley, S.P.E., Dulski, P., 2013. Volcanic ash reveals time-transgressive abrupt climate change during the Younger Dryas. Geology 41, 1251–1254.

Litt, T., Stebich, M., 1999. Bio- and chronostratigraphy of the lateglacial in the Eifel region, Germany. Quat. Int. 61, 5–16.

Litt, T., Brauer, A., Goslar, T., Merkt, J., Bałaga, K., Müller, H., Ralska-Jasiewiczowa, M., Stebich, M., Negendank, J.F.W., 2001. Correlation and synchronisation of Lateglacial continental sequences in northern central Europe based on annually laminated lacustrine sediments. Quat. Sci. Rev. 20, 1233–1249.

Litt, T., Schmincke, H., Kromer, B., 2003. Environmental response to climatic and volcanic events in central Europe during the Weichselian Lateglacial. Quat. Sci. Rev. 22, 7–32.

Liu, B., Chen, S., Liu, H., Guan, Y., 2020. Changes in the ratio of benthic to planktonic diatoms to eutrophication status of Muskegon Lake through time: implications for a valuable indicator on water quality. Ecol. Indicat. 114, 106284.

Lohne, Ø.S., Mangerud, J., Birks, H.H., 2014. IntCal13 calibrated ages of the Vedde and Saksunarvatn ashes and the younger Dryas boundaries from Kråkenes, western Norway. J. Quat. Sci. 29, 506–507.

Lotter, A.F., Bigler, C., 2000. Do diatoms in the Swiss Alps reflect the length of ice-cover? Aquat. Sci. 62, 125–141.

Lotter, A., Eicher, U., Siegenthaler, U., Birks, H., 1992. Late-glacial climatic oscillations as recorded in Swiss lake sediments. J. Quat. Sci. 7, 187–204.

Lowe, J., Bronk Ramsey, C., Housley, R.A., Lane, C.S., Tomlinson, E.L., RESET Team, RESET Associates, 2015. The RESET project: constructing a European tephra lattice for refined synchronisation of environmental and archaeological events during the last c. 100 ka. Quat. Sci. Rev. 118, 1–17.

Mangerud, J., 2021. The discovery of the Younger Dryas, and comments on the current meaning and usage of the term. Boreas 50, 1–5.

Manzano, S., Julier, A.C.M., Dirk, C.J., Razafimanantsoa, A.H.I., Samuels, I., Petersen, H., Gell, P., Hoffman, M.T., Gillson, L., 2020. Using the past to manage the future: the role of palaeoecological and long-term data in ecological restoration. Restor. Ecol. 28, 1335–1342.

Martin-Puertas, C., Matthes, K., Brauer, A., Muscheler, R., Hansen, F., Petrick, C., Aldahan, A., Possnert, G., van Geel, B., 2012. Regional atmospheric circulation shifts induced by a grand solar minimum. Nat. Geosci. 5, 397–401.

Martinez-Sosa, P., Tierney, J.E., Stefanescu, I.C., Dearing Crampton-Flood, E., Shuman, B.N., Routson, C., 2021. A global Bayesian temperature calibration for lacustrine brGDGTs. Geochem. Cosmochim. Acta 305, 87–105.

Matthias, I., Giesecke, T., 2014. Insights into pollen source area, transport and deposition from modern pollen accumulation rates in lake sediments. Quat. Sci. Rev. 87, 12–23.

McManus, J.F., Francois, R., Gherardi, J.-M., Kelgwin, L.D., Brown-Leger, S., 2004. Collapse and rapid resumption of Atlantic meridional circulation linked to deglacial climate changes. Nature 428, 834–837.

Meinke, K., 1992. Die Entwicklung der Weser im nordwestdeutschen Flachland während des jüngeren Pleistozäns. Dissertation University, Göttingen, Göttingen, Germany.

Merkt, J., Müller, H., 1999. Varve chronology and palynology of the lateglacial in northwestnorthwest Germany from lacustrine sediments of Hämelsee in lower Saxony. Quat. Int. 61, 41–59.

Moore, P.D., Webb, J.A., Collinson, M.E., 1991. Pollen Analysis. Blackwell Publishing, Oxford.

Mudelsee, M., 2019. Trend analysis of climate time series: a review of methods. Earth Sci. Rev. 190, 310–322.

Muggeo, V.M.R., 2008. segmented: an R Package to fit regression models with broken-line relationships. R. News 8/1, 20–25. https://cran.r-project.org/doc/Rnews/.

Müller, D., Tjallingii, R., Płóciennik, M., Luoto, T.P., Kotrys, B., Plessen, B., Ramisch, A., Schwab, M.J., Błaszkiewicz, M., Słowiński, M., Brauer, A., 2021. New insights into lake responses to rapid climate change: the Younger Dryas in Lake Gościąż, central Poland. Boreas 50, 535–555.

Muschitiello, F., Pausata, F.S.R., Watson, J.E., Smittenberg, R.H., Salih, A.A.M., Brooks, S.J., Whitehouse, N.J., Karlatou-Charalampopoulou, A., Wohlfarth, B., 2015. Fennoscandian freshwater control on Greenland hydroclimate shifts at the onset of the Younger Dryas. Nat. Commun. 6, 8939.

Oksanen, J., Blanchet, F.G., Friendly, M., Kindt, R., Legendre, P., McGlinn, D., Minchin, P.R., O'Hara, R.B., Simpson, G.L., Solymos, P., Stevens, M.H.H., Szoecs, E., Wagner, H., 2019. Vegan: community ecology package. R package version 2, 5–6. https://CRAN.R-project.org/package=vegan.

Płóciennik, M., Self, A., Birks, H.J.B., Brooks, S.J., 2011. Chironomidae (Insecta: Diptera) succession in Żabieniec bog and its palaeo-lake (central Poland) during the late Weichselian and Holocene. Palaeogeogr. Palaeoclimatol. Palaeoecol. 307, 150–167.

Rach, O., Brauer, A., Wilkes, H., Sachse, D., 2014. Delayed hydrological response to Greenland cooling at the onset of the younger Dryas in western Europe. Nat. Geosci. 7, 109–112.

Rach, O., Hadeen, X., Sachse, D., 2020. An automated solid phase extraction procedure for lipid biomarker purification and stable isotope analysis. Org. Geochem. 142, 103995.

Rasmussen, S.O., Bigler, M., Blockley, S.P., Blunier, T., Buchardt, S.L., Clausen, H.B., Cvijanovic, I., Dahl-Jensen, D., Johnsen, S.J., Fischer, H., Gkinis, V., Guillevic, M., Hoek, W.Z., Lowe, J.J., Pedro, J.B., Popp, T., Seierstad, I.K., Steffensen, J.P., Svensson, A.M., Vallelonga, P., Vinther, B.M., Walker, M.J.C., Wheatley, J.J., Winstrup, M., 2014. A stratigraphic framework for abrupt climatic changes during the Last Glacial period based on three synchronized Greenland ice-core records: refining and extending the INTIMATE event stratigraphy. Quat. Sci. Rev. 106, 14–28.

Reinig, F., Wacker, L., Jöris, O., Guidobaldi, G., Nievergelt, D., Adolphi, F., Cherubini, P., Engels, S., Esper, J., Land, A., Lane, C., Oppenheimer, C., Pfanz, H., Remelle, S., Sigl, M., Sookdeo, A., Büntgen, U., 2021. Precise date of the Laacher See eruption shifts onset of the Younger Dryas back in time. Nature 595, 66–69.

Ripple, W.J., Wolf, C., Newsome, T.M., Galetti, M., Alamgir, M., Crist, E., Mahmoud, M. I., Laurance, W.F., 2017. World scientists' warning to humanity: a second notice. Bioscience 67, 1026–1028.

Rockström, J., Steffen, W., Noone, K., Persson, Å., Chapin III, F.S., Lambin, E.F., Lenton, T.M., Scheffer, M., Folke, C., Schellnhuber, H.J., Nykvist, B., de Wit, C.A., Hughes, T., van der Leeuw, S., Rodhe, H., Sörlin, S., Snyder, P.K., Costanza, R., Svedin, U., Falkenmark, M., Karlberg, L., Corell, R.W., Fabry, V.J., Hansen, J., Walker, B., Liverman, D., Richardson, K., Crutzen, P., Foley, J.A., 2009. A safe operating space for humanity. Nature 461, 472–475.

RStudio Team, 2020. RStudio. Integrated Development for R. RStudio, PBC, Boston, MA. URL. http://www.rstudio.com/.

Ryves, D.B., Anderson, N.J., Flower, R.J., et al., 2013. Diatom taphonomy and silica cycling in two freshwater lakes and their implications for inferring past lake productivity. J. Paleolimnol. 49, 411–430.

Sachse, D., Billault, I., Bowen, G.J., Chikaraishi, Y., Dawson, T.E., Feakins, S.J., Freeman, K.H., Magill, C.R., McInerney, F.A., van der Meer, M.T.J., Polissar, P., Robins, R.J., Sachs, J.P., Schmidt, H.-L., Sessions, A.L., White, J.W.C., West, J.B., Kahmen, A., 2012. Molecular paleohydrology: interpreting the hydrogen-isotopic composition of lipid biomarkers from photosynthesizing organisms. Annu. Rev. Earth Planet Sci. 40, 221–249.

Schmera, D., Heino, J., Podani, J., Eros, T., Dolédec, S., 2017. Functional diversity: a review of methodology and current knowledge in freshwater macroinvertebrate research. Hydrobiologia 787, 27–44.

Schouten, S., Hopmans, E.C., Damsté, J.S.S., 2013. The organic geochemistry of glycerol dialkyl glycerol tetraether lipids: A review. Org. Geochem. 54, 19–61.

Simpson, G., 2020. Analogue: analogue and weighted averaging methods for palaeoecology. R package version (0.17–4). https://cran.r-project.org/web/packages/analogue/analogue.pdf.

Słowiński, M., Zawiska, I., Ott, F., Noryśkiewicz, A.M., Plessen, B., Apolinarska, K., Rzodkiewicz, M., Michczyńska, D.J., Wulf, S., Skubała, P., Kordowski, J., Błaszkiewicz, M., Brauer, A., 2017. Differential proxy responses to late Allerød and early Younger Dryas climatic change recorded in varved sediments of the Trzechowskie palaeolake in Northern Poland. Quat. Sci. Rev. 158, 94–106.

Smol, J.P., Wolfe, A.P., Birks, H.J.B., Douglas, M.S.V., Jones, V.J., Korhola, A., Pienitz, R., Rühland, K., Sorvari, S., Antoniades, D., Brooks, S.J., Fallu, M.-A., Hughes, M., Keatley, B.E., Laing, T.E., Michelutti, N., Nazarova, L., Nyman, M., Paterson, A.M., Perren, B., Quinlan, R., Rautio, M., Saulnier-Talbot, E., Siitonen, S., Solovieva, N., Weckström, J., 2005. Climate-driven Regime Shifts in the Biological Communities of Arctic Lakes, 102. Proceedings of the National Academy of Sciences, pp. 4397–4402.

Steffen, W., Richardson, K., Rockström, J., Cornell, S.E., Fetzer, I., Bennett, E.M., Biggs, R., Carpenter, S.R., de Vries, W., de Wit, C., Folke, C., Gerten, D., Heinke, J., Mace, G.M., Persson, L.M., Ramatnathan, V., Reyers, B., Sörlin, S., 2015. Planetary boundaries: guiding human development on a changing planet. Science 347, 1259855.

Steffensen, J.P., Andersen, K.K., Bigler, M., Clausen, H.B., Dahl-Jensen, D., Fischer, H., Goto-Azuma, K., Hansson, M., Johnsen, S.J., Jouzel, J., Masson-Delmotte, V., Popp, T., Rasmussen, S.O., Röthlisberger, R., Ruth, U., Stauffer, B., Siggaard-Andersen, M.-L., Sveinbjörnsdóttir, Á.E., Svensson, A., White, J.W.C., 2008. High-resolution Greenland ice core data show abrupt climate change happens in few years. Science 321, 680–684.

Stockmarr, J., 1971. Tablets with spores used in absolute pollen analysis. Pollen Spores 13, 615–621.

Turner, F., Pott, R., Schwarz, A., Schwalb, A., 2014. Response of Pediastrum in German floodplain lakes to Late Glacial climate changes. J. Paleolimnol. 52, 293–310.

Turner, F., Zhu, L., Lü, X., Peng, P., Ma, Q., Wang, J., Hou, J., Lin, Q., Yang, R., Frenzel, P., 2016. Pediastrum sensu lato (Chlorophyceae) assemblages from surface sediments of lakes and ponds on the Tibetan Plateau. Hydrobiologia 771, 101–118.

Turney, C.S.M., Van Den Burg, K., Wastegård, S., Davies, S.M., Whitehouse, N.J., Pilcher, J.R., Callaghan, C., 2006. North European last glacial–interglacial transition (LGIT; 15–9 ka) tephrochronology: extended limits and new events. J. Quat. Sci. 21, 335–345.

van den Bos, V., Engels, S., Bohncke, S.J.P., Cerli, C., Jansen, B., Kalbitz, K., Peterse, F., Renssen, H., Sachse, D., 2018. Late Holocene changes in vegetation and atmospheric circulation at Lake Uddelermeer (The Netherlands) reconstructed using lipid biomarkers and compound specific δD analysis. J. Quat. Sci. 33, 100–111.

Wagner-Cremer, F., Lotter, A.F., 2011. Spring-season changes during the late Pleniglacial and Bølling/Allerød interstadial. Quat. Sci. Rev. 30, 1825–1828.

Walker, M., Johnsen, S., Rasmussen, S.O., Steffensen, J.P., Popp, T., Gibbard, P., Hoek, W., Lowe, J., Andrews, J., Bjorck, S., Cwynar, L., Hughen, K., Kershaw, P., Kromer, B., Litt, T., Lowe, D.J., Nakagawa, T., Newnham, R., Schwander, J., 2008. The global Stratotype section and point (GSSP) for the base of the Holocene series/Epoch (quaternary system/period) in the NGRIP ice core. Episodes 31, 264–267.

Weber, J., Bauersachs, T., Schwark, L., 2020. A multiphasic Younger Dryas cold period recorded in sediments of Lake Steisslingen, SW-Germany: a biomarker perspective. Quat. Int. 542, 121–136.

Weijers, J.W.H., Schefuß, E., Schouten, S., Sinninghe Damsté, J.S., 2007. Coupled thermal and hydrological evolution of tropical Africa over the last deglaciation. Science 315, 1701–1704.

Weltje, G.J., Tjallingii, R., 2008. Calibration of XRF core scanners for quantitative geochemical logging of sediment cores: theory and application. Earth Planet Sci. Lett. 274, 423–438.

Willis, K.J., Birks, H.B.J., 2006. What is natural? The need for a longterm perspective in biodiversity conservation. Science 314, 1261–1265.

Wohlfarth, B., Muschitiello, F., Greenwood, S.L., Andersson, A., Kylander, M., Smittenberg, R.H., Steinthorsdottir, M., Watson, J., Whitehouse, N.J., 2017. Hässeldala – a key site for Last Termination climate events in northern Europe. Boreas 46, 143–161.

Wohlfarth, B., Luoto, T.P., Muschitiello, F., Väliranta, M., Björck, S., Davies, S.M., Kylander, M., Ljung, K., Reimer, P.J., Smittenberg, R.H., 2018. Climate and environment in southwest Sweden 15.5–11.3 cal. ka BP. Boreas 47, 687–710.

Wulf, S., Dräger, N., Ott, F., Serb, J., Appelt, O., Guðmundsdóttir, E., van den Bogaard, C., Słowiński, M., Błaszkiewicz, M., Brauer, A., 2016. Holocene tephrostratigraphy of varved sediment records from lakes Tiefer See (NE Germany) and Czechowskie (N Poland). Quat. Sci. Rev. 132, 1–14.